Copy 1

RM A56H08

NACA RM A56H08

CONFIDENTIAL

NACA

RESEARCH MEMORANDUM

LARGE-SCALE WIND-TUNNEL TESTS OF AN AIRPLANE MODEL WITH A 45° SWEPTBACK WING OF ASPECT RATIO 2.8 WITH AREA SUCTION APPLIED TO TRAILING-EDGE FLAPS AND WITH SEVERAL WING LEADING-EDGE MODIFICATIONS

By David G. Koenig and Kiyoshi Aoyagi

Ames Aeronautical Laboratory
Moffett Field, Calif.

CLASSIFIED DOCUMENT

This material contains information affecting the National Defense of the United States within the meaning of the espionage laws, Title 18, U.S.C., Secs. 793 and 794, the transmission or revelation of which in any manner to an unauthorized person is prohibited by law.

NATIONAL ADVISORY COMMITTEE FOR AERONAUTICS

WASHINGTON

November 2, 1956

CONFIDENTIAL

(4)

NATIONAL ADVISORY COMMITTEE FOR AERONAUTICS

RESEARCH MEMORANDUM

LARGE-SCALE WIND-TUNNEL TESTS OF AN AIRPLANE MODEL WITH A 45° SWEPTBACK WING OF ASPECT RATIO 2.8 WITH AREA SUCTION APPLIED TO TRAILING-EDGE FLAPS AND WITH SEVERAL WING LEADING-EDGE MODIFICATIONS

By David G. Koenig and Kiyoshi Aoyagi

SUMMARY

An investigation of an airplane model was conducted to determine the effect of area-suction trailing-edge flaps and several leading-edge modifications on the aerodynamic characteristics of a 45° sweptback wing. The wing had an aspect ratio of 2.8 and a taper ratio of 0.17. The wing was tested with a small-span constant-chord flap and, to a lesser extent, with a larger span constant-percent wing-chord flap. Area suction was applied to both flaps. Leading-edge flaps and modified leading-edge contours were tested in an effort to produce adequate leading-edge stall control. A chord extension and a fence were also tested. Part of the testing was done with a horizontal tail installed above the extended wing-chord plane. The tests were made at a Reynolds number of 10×10^6.

The flap lift increments with area suction applied to the flap were within approximately 90 percent of the theory of NACA Report 1071 at low angles of attack. At high angles of attack, wing leading-edge modifications were necessary to maintain the lift effectiveness of the flaps.

It was found that with the smaller trailing-edge flap, higher maximum lifts were obtained with a deflected plain leading-edge flap extending from the 40-percent semispan station to the wing tip than were obtained with full-span leading-edge flaps. The larger span trailing-edge flaps produced a maximum lift only slightly higher than was obtained with the small trailing-edge flap.

The highest values of tail-off maximum lift coefficient for the smaller trailing-edge flap deflected 60° with suction, which were of the order of 1.45, were obtained with the part-span leading-edge flap deflected 30° or 40° and with a modified leading edge (obtained by combining leading-edge camber with increased leading-edge radii of

either 0.9- or 1.8-percent chord). Reducing the size of the modified leading edge from a leading-edge radius of 1.8- to 0.9-percent chord did not effect maximum lift with the leading-edge flap deflected but produced some reduction when the leading-edge flap was undeflected.

With the horizontal tail installed, none of the wing modifications proved satisfactory in alleviating adverse pitching-moment variations in the medium to high lift range. These adverse pitching-moment variations were reduced by drooping the horizontal tail.

INTRODUCTION

Boundary-layer control as a means of preventing flow separation has been found an effective means of augmenting flap lift effectiveness. Results of tests of a large-scale wind-tunnel model with a 35° swept wing and with area suction applied to the trailing-edge flaps are reported in references 1 and 2. To control leading-edge air-flow separation, area suction was effectively applied both at the knee of the leading-edge flap and at the wing leading edge, as reported in references 2 and 3, respectively. Flight tests of an airplane with a wing similar to that of the wind-tunnel model and with area suction applied at the knee of the trailing-edge flap are reported in reference 4 and results are presented in reference 5 for the airplane equipped with an area-suction leading edge. A less extensive study reported in reference 6 was made of the application of area suction to the trailing-edge flaps of a large-scale triangular-wing model of thin wing section. In this investigation, no effort was made to control leading-edge air-flow separation which reduced the flap lift effectiveness at high angles of attack.

As an extension of the boundary-layer control program in the Ames 40- by 80-foot wind tunnel, an investigation was undertaken on an airplane model with a plan form between that of the 35° swept wing and that of the triangular-wing model in regard to aspect ratio, sweep, and taper ratio. Because of its similarity to that of a recent design proposal, the plan form chosen was of aspect ratio 2.8, taper ratio 0.17 with the quarter-chord line swept back 45°.

The investigation included the determination of the lift effectiveness of area-suction flaps on the model, as well as the study of the effect of the loading induced by the flap on the progression of flow separation on the wing. Several wing modifications were investigated as means of controlling leading-edge air-flow separation. A portion of the investigation was concerned with a study of the aerodynamic characteristics of the model with a horizontal tail installed.

NOTATION

A	aspect ratio, $\frac{b^2}{S}$
b	wing span, ft
c	chord, measured parallel to the plane of symmetry, ft
c'	chord, measured normal to the wing leading edge, ft
$\bar{c}$	mean aerodynamic chord, $\frac{2}{S}\int_0^{b/2} c^2 dy$, ft
C_D	drag coefficient, $\frac{\text{drag}}{q_\infty S}$
C_L	lift coefficient, $\frac{\text{lift}}{q_\infty S}$
C_m	pitching-moment coefficient computed about the quarter-chord point of the mean aerodynamic chord, $\frac{\text{pitching moment}}{q_\infty S\bar{c}}$
C_Q	flow coefficient, $\frac{Q}{U_\infty S}$
d	chordwise location of forward edge of porous surface, in.
LE	leading edge
l	chordwise extent of porous area, in.
l_t	distance from the quarter-chord point of the mean aerodynamic chord to horizontal-tail reference line
p_d	average duct static pressure, lb/sq ft
p_l	local surface static pressure, lb/sq ft
p_∞	free-stream static pressure, lb/sq ft
P	airfoil pressure coefficient, $\frac{p_l - p_\infty}{q_\infty}$
P_d	average duct pressure coefficient, $\frac{p_d - p_\infty}{q_\infty}$

Δp	pressure drop across porous material, lb/sq ft
q_∞	free-stream dynamic pressure, lb/sq ft
Q	volume of air removed through porous surface, cu ft/sec, based on standard density
R	radius
S	wing area, sq ft
TE	trailing edge
V_∞	free-stream velocity, ft/sec
y	perpendicular distance from plane of symmetry, ft
z	perpendicular distance above the extended wing-chord plane, ft
α	angle of attack, deg
α_δ	$\frac{d\alpha}{d\delta}$
Γ	dihedral, deg
δ	flap deflection, measured in plane normal to the hinge line, deg
η	wing semispan station, $\frac{2y}{b}$
λ	taper ratio, $\frac{\text{tip chord}}{\text{root chord}}$
Λ	sweep angle, deg

Subscripts

c	critical
f	trailing-edge flap
n	leading-edge flap
max	maximum
min	minimum

MODEL AND APPARATUS

The Model

A photograph of the model as mounted in the Ames 40- by 80-foot wind tunnel is shown in figure 1. A drawing of the model is shown in figure 2(a), and additional geometric data are given in table I. The wing of the model had a sweep of 45° and an aspect ratio of 2.8 with a taper ratio of 0.17. The airfoil sections parallel to the model symmetrical center line were modified NACA 0005-63 sections, the coordinates of which are listed in table II. The modification consisted of a straight-line fairing from the 67-percent-chord station to the trailing edge.

A small-span and large-span trailing-edge flap were used during the tests. The small-span flap had a constant chord (equivalent to 17.3-percent chord at 0.21 of the wing semispan) and spanned 0.25 of the wing semispan. The large-span flap had a constant 25-percent chord and spanned 0.45 of the wing semispan. For both flaps, the inboard ends were located at $\eta = 0.21$, the flaps rotated about a hinge near the lower wing surface, and they were equipped with porous-area suction.

The wing was combined with a slender fuselage which was somewhat underslung with respect to the wing. A side inlet duct was installed on the fuselage to simulate an engine intake configuration similar to that of a current airplane design. For a free-stream velocity of 130 feet per second, the inlet velocity ratio was approximately 0.7 and was nearly constant throughout the angle-of-attack range. The fuselage and external ducting details are shown in figure 2(b).

A swept horizontal tail was used in the investigation and was installed 0.21 of the wing semispan above the extended wing-chord plane. The tail could be drooped about a hinge line close to the plane of symmetry and parallel to it and the extended wing-chord plane.

Boundary-Layer Control System

Duct and pumping system.- The suction system employed on the trailing-edge flaps is shown in figure 3(a). Air was drawn from the flap through the wing ducts and plenum chamber into the blower, and then was exhausted through the exhaust duct beneath the fuselage. The pump was a modified aircraft engine supercharger driven by a variable-speed electric motor. The flow quantity was obtained by measuring the pressure difference between the plenum chamber and the inlet pipe to the blower. This system was calibrated against standard ASME intake orifices. Wing duct pressure measurements were obtained from static-pressure taps inside the duct located at 0.25, 0.37, 0.52, and 0.62 of the wing semispan.

Porous surface.- The flaps were constructed with a porous surface in the vicinity of the knee of the flap as shown in figure 3(b). The chordwise extent and position of the porous opening were controlled by covering portions of the porous material with a nonporous tape approximately 0.003 inch thick. The porous openings used in the tests are listed in table III. The porous material used was composed of an electroplated metal mesh sheet backed with 1/16-inch-thick white wool felt. The metal mesh sheet was 0.008 inch thick, 11-percent porous, and had 4225 holes per square inch. The permeability of the felt with the metal mesh sheet is shown in figure 3(c).

Wing Modifications

During the investigation, several types of wing modifications were installed as shown in figure 4.

Leading-edge flap.- Part-span and full-span leading-edge flaps extended from the wing tip inboard to 0.40 and 0.21 of the wing semispan, respectively. The flaps were hinged near the lower wing surface at 12-percent c.

Modified leading edges.- Changes in leading-edge contour[1] were made by increasing the leading-edge radius to approximately 0.9 and 1.8 percent of the wing chord (normal to the leading edge) and adding a small amount of leading-edge camber, such that the center of the leading-edge arcs were, respectively, 0.9- and 1.7-percent c' below the wing chord plane. The modified leading edge (leading-edge radius 0.9-percent c') extended from 0.40 of the wing semispan to the tip. In addition, a leading-edge contour which tapered linearly from the plain leading edge at 0.40 of the wing semispan to the smaller modified leading edge (leading-edge radius 0.9-percent c') at 0.60 of the wing semispan was investigated. Two spans of the modified leading edge (leading-edge radius 1.8-percent c') were used which extended from the wing tip inboard to 0.40 and 0.21 of the wing semispan.

The modified leading edges were made of sheetmetal wrapped around wooden ribs which were fitted to the plain leading edge. The flexibility of the sheetmetal used impaired accuracy in maintaining the contour. However, the results obtained for the profiles with the sheetmetal and wood rib construction are believed representative of those possible with accurately contoured leading-edge profiles.

[1]Leading-edge radius of plain wing perpendicular to wing leading edge was 0.36-percent c'.

Chord extensions.- Two leading-edge chord extensions, extending from 0.60 semispan to the wing tip, were installed on the wing with the part-span plain leading-edge flap (η = 0.4 to 1.0) deflected. The plain chord extension extended forward approximately 10 percent of the wing chord measured parallel to the model plane of symmetry; the second chord extension was constructed by modifying the leading edge of the plain chord extension to a radius of 0.90 percent of the wing chord (normal to the wing leading edge) and adding a small amount of camber. The chord extensions hereinafter will be referred to as chord extensions A and B, respectively. Both chord extensions were constructed with sheetmetal and wooden ribs.

Fence.- A test was made with a full-chord fence 7.0-percent c high located on the wing at 0.70 of the wing semispan parallel to the plane of symmetry of the model.

TESTING AND PROCEDURE

Force, moment, and pressure data were obtained for the model through an angle-of-attack range of -4° to 28°. The model configurations for which force and moment data were obtained are listed in table IV which also may be used as an index to the basic data. All tests, except for the brief tests at higher free-stream velocities with variable suction flow quantities (as will be mentioned), were made at a Reynolds number of 10×10^6, based on the mean aerodynamic chord. This Reynolds number corresponded to a free-stream dynamic pressure of 20 pounds per square foot and a Mach number of 0.11.

Tests at Variable Angle of Attack

Data were obtained for the plain leading edge with the side inlet duct either off or on and the small-span trailing-edge flap at 0°, 50°, and 60° deflections with and without area suction. A major part of the testing was devoted to the investigation of various wing modifications for improvement of high lift characteristics of the model, mainly with the small-span trailing-edge flap deflected 60°. During the investigation, full-span and part-span leading-edge flaps were deflected 0°, 30°, or 40°, and a 15° deflection was tested only for the part-span flap. The modified leading edges were tested with and without the leading-edge flap deflected in combination with the small trailing-edge flap either undeflected or deflected 60°.

The chord extensions were tested only with the part-span plain leading-edge flap deflected 40°. The fence was investigated with the same wing and tail configuration as the chord extensions except that

the modified leading edge (leading-edge radius 0.9-percent c) was installed on the leading-edge flap. For all tests with chord extensions or fences, the horizontal tail was installed and the small-span trailing-edge flap was deflected 60° with suction.

The large-span trailing-edge flap was tested only briefly with the flap deflected 60° with suction in combination with the part-span plain leading-edge flap deflected 40°.

All testing at variable angles of attack with area suction was done at a constant blower speed with porous surface numbers 1 and 8 (see table III) with the small-span flap deflected 50° and 60°, respectively, and with the porous-surface configuration described in table III for the model with the large-span flap deflected. The blower speed was set to produce an approximately constant flow quantity about twice that of the critical flow quantity required for the same porous-surface configuration at zero angle of attack.

Tests were made with the horizontal tail installed on the model with the flaps deflected for several wing modifications. Data were obtained with the tail drooped at dihedrals of 0°, -15°, -20°, and -25°.

Tests With Variable Suction Flow at Constant Angle of Attack

Suction flow quantities were varied for given angles of attack and free-stream velocities to determine actual suction requirements for various porous-area configurations. For all of the porous-area configurations tested, data were obtained with decreasing values of C_Q. To investigate hysteresis effects for several of the porous openings, data were obtained with increasing values of C_Q, but for each of these cases the hysteresis effects were negligible.

The various extents and positions of porous areas tested are listed in table III. For the model with the small-span flap deflected 60° and with porous area 8 (table III), tests were made at nominal angles of attack of 0°, 8°, 16°, and 20°. For the remaining configurations, tests were made at an uncorrected angle of attack of zero. Additional tests to determine the effect of free-stream velocity on the suction flow requirements were made for a particular model configuration and one porous-area configuration. These tests were made at approximately zero angle of attack and free-stream velocities of 114, 162, and 186 feet per second, corresponding to Reynolds numbers of 8.7, 12.2, and 14.2×10^6, respectively, based on the mean aerodynamic chord of the wing.

CORRECTIONS TO DATA

All data were corrected for air-stream inclination and for wind-tunnel wall effects, the latter correction being that for a wing of the same span having elliptic loading but with an unswept plan form. This procedure was followed since an analysis indicated that tunnel-wall corrections were approximately the same for straight and swept wings of the size under consideration. These corrections were made as follows:

$$\Delta\alpha = 0.75\ C_L$$

$$\Delta C_D = 0.013\ C_L^2$$

For the data with the horizontal tail installed, a correction for additional downwash at the hinge line of the tail (at the model plane of symmetry) was made as follows:

$$\Delta C_{m_T} = 0.0124\ C_L$$

This correction depends on tail effectiveness but the values of ΔC_{m_T} corresponding to the tail effectiveness of the undrooped tail were used with the data for both the undrooped and drooped tails.

Drag and pitching-moment tares due to strut interference based on data obtained with a rectangular wing were applied to the data. These corrections do not include the probable effects of additional installations on the mounting struts which were necessary for the present investigation.

All flow coefficients were corrected to standard sea-level air conditions and are believed accurate to within ±4 percent. The effect of the thrust of the exhaust jets on the aerodynamic data was negligible.

RESULTS AND DISCUSSION

The model configurations for which force and moment data are presented are listed in table IV which may also be used as an index to figures 5 through 15. Chordwise pressure distributions are presented in figures 16 and 17 for the model without and with the part-span leading-edge flaps (η = 0.40 to 1.0) deflected.

Effect of Trailing-Edge Flaps on the Aerodynamic Characteristics of the Model With Horizontal Tail Off

Characteristics at 0° angle of attack.- To show the effectiveness of the trailing-edge flaps, flap lift increments obtained at $\alpha = 0^\circ$, ΔC_{L_f}, for both the large- and small-span flaps are presented in the following table:

Side inlet duct	δ_f, deg	ΔC_{L_f} suction		ΔC_{L_f} theory, reference 7	Percent theory, suction on	Figures from which experimental values were derived
		Off	On			
Small-span flap						
Off	50	0.29	0.37	0.40	93	5(a) and (b)
Off	60	.29	.41	.48	86	5(a) and (b)
On	60	.27	.44	.48	92	7
Large-span flap						
On	60		.76	.88	86	7(a) and 13

For determining the theoretical values of flap lift increment, the method of reference 7 was applied and the theoretical values of α_δ presented in figure 3 of that reference were used.

Characteristics in the moderate to high lift-coefficient range.- As may be seen from figure 5, for angles of attack from 0° to 10°, the flap lift increment for the small-span flap with area suction remained constant. Above 10° the flap lift increment decreased. In addition to the loss in flap lift, destabilizing variations in pitching moment started just before the loss in flap lift occurred and became more severe at higher angles of attack.

The data presented in figure 6 indicate that, generally, only small changes in the aerodynamic characteristics resulted when the external side-inlet duct was installed. However, with the duct on, the unstable variation in pitching moment was somewhat more abrupt.

Tuft observations and the pressure data of figure 16 show that the adverse stability changes and the reduction in flap lift were the result of stall due to leading-edge air-flow separation which first appeared at the wing tips and then moved inboard with further increase in angle of attack. The fact that increased loading on the wing due to higher flap effectiveness, as obtained by application of boundary-layer control, aggravated leading-edge air-flow separation is shown by the effects of suction on the wing pressure distributions of figure 16, particularly at 8° and 12°

angle of attack. It is believed that these effects are the same as would result from increasing the flap lift by increasing the flap deflection with adequate boundary-layer control.

The Effect of Wing Modifications on the High-Lift Characteristics of the Model With the Horizontal Tail Off

A summary of the lift and pitching-moment characteristics of the tail-off model for several wing modifications is presented in figure 18 for the model with the small-span flap deflected 60° and with area suction.

The following table is a list of tail-off values of $C_{L_{max}}$ for several wing modifications for the model with the small-span flap deflected 60° and with area suction (η = 0.21 to 0.46). These values of $C_{L_{max}}$ listed represent the value of C_L at which the slope of the lift curve first became zero.

Leading edge		Leading-edge flap		$C_{L_{max}}$	α, deg	Figure
Type	Extent, η	δ_n, deg	Extent, η			
Plain		0		1.07	20	7(c)
Plain		40	0.4 to 1.0	1.32	21	7(c)
Plain		40	0.21 to 1.0	1.18	18	7(c)
1.8-percent LER	0.4 to 1.0	0	0.4 to 1.0	1.29	21	11
1.8-percent LER	0.4 to 1.0	30	0.4 to 1.0	1.46	25	11
1.8-percent LER	0.21 to 1.0	0	0.4 to 1.0	1.19	19	11
1.8-percent LER	0.21 to 1.0	30	0.4 to 1.0	1.34	22	11

For the model with the larger-span trailing-edge flap deflected, tuft and pressure observations indicated that the higher loading on the wing due to the flap, as compared to that obtained with the small-span flap, produced leading-edge air-flow separation and consequent flow separation over the outboard portion of the flap at lower angles of attack. This contributed to the early loss in flap lift shown by the data of figure 13 and, for the wing modifications investigated (plain leading edge, δ_n = 40°, with η = 0.40 to 1.0), this early flap stall limited $C_{L_{max}}$ to values only slightly larger than those obtained with the small-span flap.

Since most of the wing modifications tested were in combination with the small-span trailing-edge flap, the following discussion concerning the effectiveness of each wing modification will therefore be based on these tests.

Leading-edge flap with plain wing leading edge.- As is shown by pitching-moment data of figure 7, the effect of deflecting the full-span plain leading-edge flap with and without suction on the trailing-edge flap was to delay the loss in lift at the tip, as indicated by an abrupt destabilizing change in stability. When tip stall did occur with the leading-edge flap deflected to values of $\delta_n = 30^\circ$ or 40°, as indicated by both tuft observations and pressure measurements (see fig. 17), it was evidently precipitated by leading-edge flow separation. This happened in spite of the fact that local flow separation aft of the knee of the leading-edge flap occurred approximately 2° angle of attack earlier than leading-edge air-flow separation. After the onset of tip stall, the rate at which air-flow separation at the leading-edge flap knee and subsequent complete stall of the wing sections moved inboard was approximately the same as was found for the model without the leading-edge flaps deflected.

With the part-span leading-edge flap, as may be seen in figures 7(b) and (c), higher lifts were obtained above 14° to 16° than with the full-span flap for the model with the trailing-edge flap deflected. However, the angle of attack at which the adverse and abrupt pitching-moment variation occurred was unchanged from that obtained with the full-span leading-edge flap. From pressure measurements (not presented herein) as well as tuft observations, it was found that with the part-span leading-edge flap, the higher values of $C_{L_{max}}$ may be attributed to a reduction in the rate of stall progression from $\eta = 0.60$ inboard. This reduction in the rate of the stall progression helped in maintaining trailing-edge flap lift up to higher angles of attack.

Figure 19 shows the variations of $C_{L_{max}}$ with δ_n. It might be concluded from the linearity of the curve for the higher values of δ_n that, for the plain leading edge, no adverse effect on maximum lift was caused by the area of separated flow behind the leading-edge flap knee.

Increased leading-edge radius combined with leading-edge camber.- From the preceding phases of the investigation, it is clear that stall on the plain wing (with or without trailing-edge flaps) was initiated by leading-edge air-flow separation which also limited the stall-control effectiveness of the leading-edge flaps. To control the leading-edge air-flow separation, two principal leading-edge contour modifications were investigated which combined some leading-edge camber with leading-edge radii of 0.9- and 1.8-percent c'.

For the wing without leading-edge flaps, the modified leading edge (leading-edge radius 1.8-percent c') as installed on the wing from $\eta = 0.40$ to the wing tip was about as effective as the part-span plain leading-edge flap. However, as shown by the data of figure 9(a), reducing the size of the modified leading edge from a leading-edge radius of 1.8-percent c' to 0.9 substantially reduced $C_{L_{max}}$.

For the model with the trailing-edge flaps deflected (suction on), with the part-span leading-edge flap deflected, and with either of the modified leading edges installed on the deflected wing leading edge (η = 0.40 to 1.0), values of $C_{L_{max}}$ of the order of 1.45 were obtained. As may be seen from figure 9(b) with the leading-edge flaps deflected, reducing the size of the modified leading edge to 0.9 percent did not reduce the maximum lift of the model.

As may be seen from figure 10, with the leading-edge flap deflected 30° or 40°, installation of the modified leading edge did not change the angle of attack at which abrupt stability changes occurred. Tuft observations showed that the leading-edge modification with leading-edge radius 1.8-percent c' (for both spanwise extents) delayed the onset of leading-edge air-flow separation at the tips to α = 17°, but that the change in stability evidently originated from a growing area of flow separation behind the leading-edge flap knee. The data of figure 19 for the modified leading-edge radius 1.8-percent c' show that little increase in $C_{L_{max}}$ could be obtained with leading-edge flap deflections higher than 30°. It is believed that this is also the result of chordwise expansion of the area of flow separation behind the leading-edge flap knee with increasingly high values of δ_n. Preventing or limiting this air-flow separation by applying boundary-layer control at the leading-edge flap knee would probably increase $C_{L_{max}}$ and delay the stability change to higher angles of attack for the model with the 40° deflected leading-edge flap. In addition, boundary-layer control would probably make effective use of higher leading-edge flap deflection possible.

The change in aerodynamic characteristics with a change in spanwise extent of the modified leading edge (leading-edge radius 1.8-percent c') is shown by the data presented in figure 11. These data show that higher maximum lifts are obtained by using the part-span (η = 0.40 to 1.0) modification, either with or without the leading-edge flap (η = 0.40 to 1.0) deflected, than by using the full-span modification for a given trailing-edge flap configuration. In addition, it is evident that tapering the leading-edge contour from the contour of the plain wing at η = 0.40 to that of the modified leading edge (leading-edge radius 0.9-percent c') at η = 0.60 with no leading-edge modification between η = 0.21 and 0.4 had little deleterious effect on the force and moment characteristics. However, from pressure measurements (not presented herein), it was observed that for wing stations inboard of η = 0.75, leading-edge air-flow separation occurred somewhat earlier than for the untapered leading-edge modification.

Chord extensions and fence.- The tests on the model equipped with chord extensions and wing fences were made principally to check their effectiveness in improving stability for the model with horizontal tail on. Consequently, the tail-off data obtained are insufficient to enable a complete comparison of lift characteristics with those obtained from

other wing modifications. However, a comparison of the tail-on data shown in figure 12 indicates that adding the chord extension A to the wing leading edge with part-span flaps (η = 0.40 to 1.0) deflected 40° produced little increase in $C_{L_{max}}$ but produced a delay in the onset of instability and presumably also delayed the tip stall. The increased leading-edge radius of 0.9-percent c' on the nose of the chord extension (chord extension B) delayed the onset of tip stall slightly and increased $C_{L_{max}}$ by 0.05. The fence was added to the wing which was already equipped with the modified leading edge (leading-edge radius 0.9-percent c' installed on the part-span, η = 0.40 to 1.0, leading-edge flap deflected 40°). As shown by the data of figure 12(a), it was found that the fence reduced $C_{L_{max}}$ but slightly delayed the onset of instability.

Aerodynamic Characteristics of the Model With the Horizontal Tail Installed

Addition of the horizontal tail did not change the angle of attack at which adverse pitching-moment variations occurred but it made them more severe than for the model with the tail off. (See figs. 10, 13, and 15.) It was found that none of the wing modifications investigated alleviated this instability satisfactorily although any modification which delayed leading-edge air-flow separation tended to diminish the severity of the instability. As mentioned previously, the use of a more effective leading-edge-stall control device such as boundary-layer control would be expected to offer promise in delaying and reducing the instability.

Previous investigations on swept-wing models such as that described in reference 8 have indicated that inward movement of the wing-tip vortices following inward movement of wing stall places definite limitations on the locations of the tail consistent with adequate longitudinal stability. This was true in particular for the aspect-ratio-2 triangular-wing model reported in reference 8. It was shown for that particular tail length that lowering the tail to positions approaching the extended wing-chord plane produced less adverse pitching-moment variations. For the present investigation, it was thought that these more favorable low tail positions might be simulated by drooping the tail and pulling it away from the adverse downwash field produced by the inward moving tip vortex trails.

As can be seen from the data of figures 12 through 15, for the model with the small-span flap, drooping the tail did cause a definite improvement in the pitching-moment variations for all of the wing modifications tested. That this improvement is similar in nature to that found for the triangular-wing model is demonstrated in figure 20. In this figure a comparison is made of the variations of ΔC_{m_T} with angle of attack for the present model (with drooped and undrooped tail) with those found for two

tail heights in the investigation of reference 8. (Data for the higher tail position presented for the previous investigation of the model of reference 8 have not been published previously.) Even though quantitatively there are wide differences between the two sets of curves due to differences in model configuration, the trends show that drooping and lowering the tail have similar effects.

Area-Suction Requirements

During the investigation it was established that the wing modifications tested had little effect on the suction air-flow requirements and, consequently, no reference will be made to wing modifications in the following presentation.

The variation of lift coefficient with flow coefficient for the small-span flap deflected 60° is shown in figures 21(a) and 21(b) for two porous openings. As indicated in figure 21(a), a critical value of flow coefficient, C_{Q_c}, exists for which larger values of C_Q produced only small gains in lift. It is evident that angle of attack had little effect on the critical flow coefficient.

The following are values of duct pressure and critical flow coefficients obtained for the small-span flap at approximately $\alpha = 0°$:

δ_f, deg	Porous surface		P_d	C_{Q_c}
	d, in.	l, in.		
50	0.8	4.1	-4.2	0.00022
60	1.0	4.4	-6.4	.00038
60	1.7	2.0	-7.9	.00022

The values shown for the 50° deflection probably do not represent minimum flow conditions since no attempt was made to reduce flow quantities for this flap deflection. For the 60° deflection, the data for the two porous-area configurations show that lower values of C_{Q_c} were obtained at the expense of somewhat more negative duct pressures.

For the large-span flap, the variation of lift coefficient with flow coefficient is shown in figure 21(c). For this flap, only one porous opening was considered and no attempt was made to reduce C_{Q_c}.

For the small-span flap, the effect of chordwise extent and location of the porous area on C_{Q_c} is shown in figure 22. It is evident that for each position of the forward edge of the porous surface (d), there was an

optimum value of porous surface extent (l), with larger or smaller values of l producing higher values of C_{Q_c}. It was also found that the forward edge could be moved aft at least to the point of bisection of the knee arc before flow requirements increased significantly or, although not shown by the data of figure 22, loss of flap lift occurred.

Figure 23 shows that the effect of free-stream velocity on the variation of C_L with C_Q for the small-span flap was negligible.

The effect of area suction on the pressure distributions near the flap knee.- The effect of flow coefficient on the chordwise pressure distribution in the vicinity of the knee of the small-span flap is shown in figure 24 for two spanwise station locations. Also shown in the figure are equivalent duct pressure coefficients for each value of C_Q for which the data are presented.

For the large-span flap, chordwise pressure distributions are shown in figure 25(a) for $\eta = 0.52$, and in figure 25(b) the spanwise variation in external minimum pressure and duct pressure coefficients are shown.

A comparison of these data with the corresponding C_L versus C_Q plots of figures 21(a) and 21(c) indicates that for C_Q values above C_{Q_c} the minimum pressure coefficient varied only slightly whereas the duct pressure variation was relatively large for both flaps.

CONCLUDING REMARKS

The results of tests on a model with a 45° sweptback wing of aspect ratio 2.8 and of taper ratio 0.17 showed that area suction was effective in increasing the flap lift increment of a small- and large-span trailing-edge flap to within about 90 percent of the theoretical value (theory of ref. 7). It was established early in the investigation, however, that the lift advantage of the flap installation was penalized greatly at high angles of attack by leading-edge air-flow separation.

Among the devices studied in an attempt to control air-flow separation from the wing leading edge, two of the devices (leading-edge flap and leading-edge flap with increased leading-edge radius) served to delay air-flow separation and thus to increase maximum lift coefficient, $C_{L_{max}}$, and reduce tail-off or tail-on instability. The highest value of $C_{L_{max}}$, however, remained limited by air-flow separation from the wing leading edge or hinge line of the leading-edge flap and favorable stability characteristics could be achieved only by a substantial effective lowering of the

horizontal tail. These results suggest that substantial gains would result from the use of boundary-layer control on the leading-edge flap which in past investigation has proved successful on other types of wing plan forms.

Ames Aeronautical Laboratory
National Advisory Committee for Aeronautics
Moffett Field, Calif., Aug. 8, 1956

REFERENCES

1. Cook, Woodrow L., Holzhauser, Curt A., and Kelly, Mark W.: The Use of Area Suction for the Purpose of Improving Trailing-Edge Effectiveness on a 35° Sweptback Wing. NACA RM A53E06, 1953.

2. Holzhauser, Curt A., and Martin, Robert K.: The Use of a Leading-Edge Area-Suction Flap to Delay Separation of Air Flow From the Leading Edge of a 35° Sweptback Wing. NACA RM A53J26, 1953.

3. Holzhauser, Curt A., and Martin, Robert K.: The Use of Leading-Edge Area Suction to Increase the Maximum Lift Coefficient of a 35° Swept-Back Wing. NACA RM A52G17, 1952.

4. Anderson, Seth B., and Quigley, Hervey C.: Flight Measurements of the Low-Speed Characteristics of a 35° Swept-Wing Airplane With Area-Suction Boundary-Layer Control on the Flaps. NACA RM A55K29, 1956.

5. Bray, Richard S., and Innis, Robert C.: Flight Tests of a Leading-Edge Area Suction Flap on a Fighter-Type Airplane With a 35° Sweptback Wing. NACA RM A55C07, 1955.

6. Kelly, Mark W., and Tolhurst, William H., Jr.: The Use of Area Suction to Increase the Effectiveness of a Trailing-Edge Flap on a Triangular Wing of Aspect Ratio 2. NACA RM A54A25, 1954.

7. DeYoung, John: Theoretical Symmetric Span Loading Due to Flap Deflection for Wings of Arbitrary Plan Form at Subsonic Speeds. NACA Rep. 1071, 1952.

8. Graham, David, and Koenig, David C.: Tests in the Ames 40- by 80-Foot Wing Tunnel of an Airplane Configuration With an Aspect Ratio 2 Triangular Wing and an All-Movable Horizontal Tail - Longitudinal Characteristics. NACA RM A51B21, 1951.

TABLE I.- GEOMETRIC DATA

Wing	
Area, sq ft	334.8
Span, ft	30.62
Mean aerodynamic chord, ft	12.77
Root chord, ft	18.69
Aspect ratio	2.8
Taper ratio	0.17
Sweep angle, deg	
Leading edge	51.7
Quarter-chord line	45.4
Trailing edge	14.2
Small-span trailing-edge flap	
Area, sq ft	10.22
Flap span, percent wing semispan (21 to 46 percent)	25.0
Constant streamwise chord, ft	2.67
Sweep angle of hinge line, deg	14.2
Large-span trailing-edge flap	
Area, sq ft	20.57
Flap span, percent wing semispan (21 to 66 percent)	45.0
Chord, percent wing chord	25.0
Sweep angle of hinge line, deg	26.8
Fuselage	
Length, ft	62.50
Maximum width, ft	4.50
Fineness ratio in wing chord plane	13.9
Horizontal tail	
S_t/S	0.204
b_t/b	0.56
$l_t/\bar{c}$	1.51
Aspect ratio	4.5
Taper ratio	0.30
Sweep angle of quarter-chord line, deg	38.4

TABLE II.- COORDINATES OF THE NACA 0005 (MODIFIED) SECTION

Station, percent chord	Ordinate, percent chord	Station, percent chord	Ordinate, percent chord
0	0	30.00	2.501
1.25	.789	40.00	2.419
2.50	1.089	50.00	2.206
5.00	1.481	60.00	1.902
7.50	1.750	67.00	1.650
10.00	1.951	70.00	1.500
15.00	2.228	80.00	1.000
20.00	2.391	90.00	.500
25.00	2.476	100.00	0
LER: 0.275-percent c			

TABLE III.- POROUS-SURFACE CONFIGURATIONS USED IN THE PRESENT INVESTIGATION

Trailing-edge flap span	η	Porous surface number	l, in.	d, in.
$\delta_f = 50^\circ$				
Small	21 to 46	1	4.1	0.8
$\delta_f = 60^\circ$				
Small	21 to 46	2	1.5	0.7
		3	2.0	
		4	3.0	
		5	4.4	
		6	2.0	1.0
		7	3.0	
		8	4.4	
		9	1.5	1.3
		10	2.0	
		11	2.5	
		12	3.0	
		13	4.4	
		14	1.0	1.7
		15	1.5	
		16	2.0	
		17	3.0	
		18	4.4	
		19	3.0	2.0
		20	4.4	2.0
Large	21[1]	---	5.4	1.4
	66	---	3.9	0.8

[1]Porous surface extent tapered linearly from η = 0.21 to 0.66.

TABLE IV.- MODEL CONFIGURATIONS FOR WHICH THREE-COMPONENT FORCE DATA ARE PRESENTED

Figure No.	Leading-edge flap		Wing leading edge		Trailing-edge flap			Side-inlet duct	Horizontal tail, Γ, deg
	δ_n, deg	Span	Contour	Span	Span	δ_f, deg	Suction		
5(a) 5(b)	0	---	Plain	---	Small[1]	0,50,60	Off On	Off	Off
6	0	---	Plain	---	Small	0,60	On	Off On	Off
7(a)	30,40	Part[2]	Plain	---	Small	0	---	On	Off
	0,30,40	Full							
7(b)	30,40	Part[2]				60	Off		
	0,30,40	Full							
7(c)	30,40	Part[2]					On		
	0,30,40	Full							
8	0 and 40	Part	Modified to LER 1.8-percent c'	Part	Small	0	---	On	Off
						60	Off On		
9(a)	0	Part	Modified to LER 1.8-percent c' Modified to LER 0.9-percent c' Plain	Part	Small	60	On	On	Off
9(b)	30	Part	Modified to LER 1.8-percent c' Modified to LER 0.9-percent c' Plain						
10	0,15,30,40	Part	Modified to LER 1.8-percent c'	Part	Small	60	On	On	Off
11	0 and 30	Part	Modified to LER 1.8-percent c'	Part	Small	60	On	On	Off
			Modified to LER 1.8-percent c'	Full					
	30		Tapered from plain at η = 0.4 to LER 0.9-percent c' at η = 0.6	Part					
12(a)	40	Part	Modified to LER 0.9-percent c' Chord extension A Chord extension B Fence plus modified LE	Part	Small	60	On	On	0
12(b)			Modified to LER 0.9-percent c' Chord extension A Chord extension B						-25
13	40	Part	Plain	---	Small	60	On	On	Off
					Large[1]				Off
					Large				0
					Large				-25
14	40	Part	Plain	---	Small	60	On	On	0,-15,-20,-25
15	40	Part	Modified to LER 0.9-percent c'	---	Small	60	On	On	0,-15,-20,-25

[1]Small-span flap extends from 21- to 46-percent semispan; large-span flap extends from 21- to 66-percent semispan.

[2]Part span for both leading-edge flap and modified leading edge refers to that extending from 40-percent semispan to wing tip and full span from 21-percent (side of inlet duct) to wing tip.

A-20739

Figure 1.- Photograph of model in the Ames 40- by 80-foot wind tunnel.

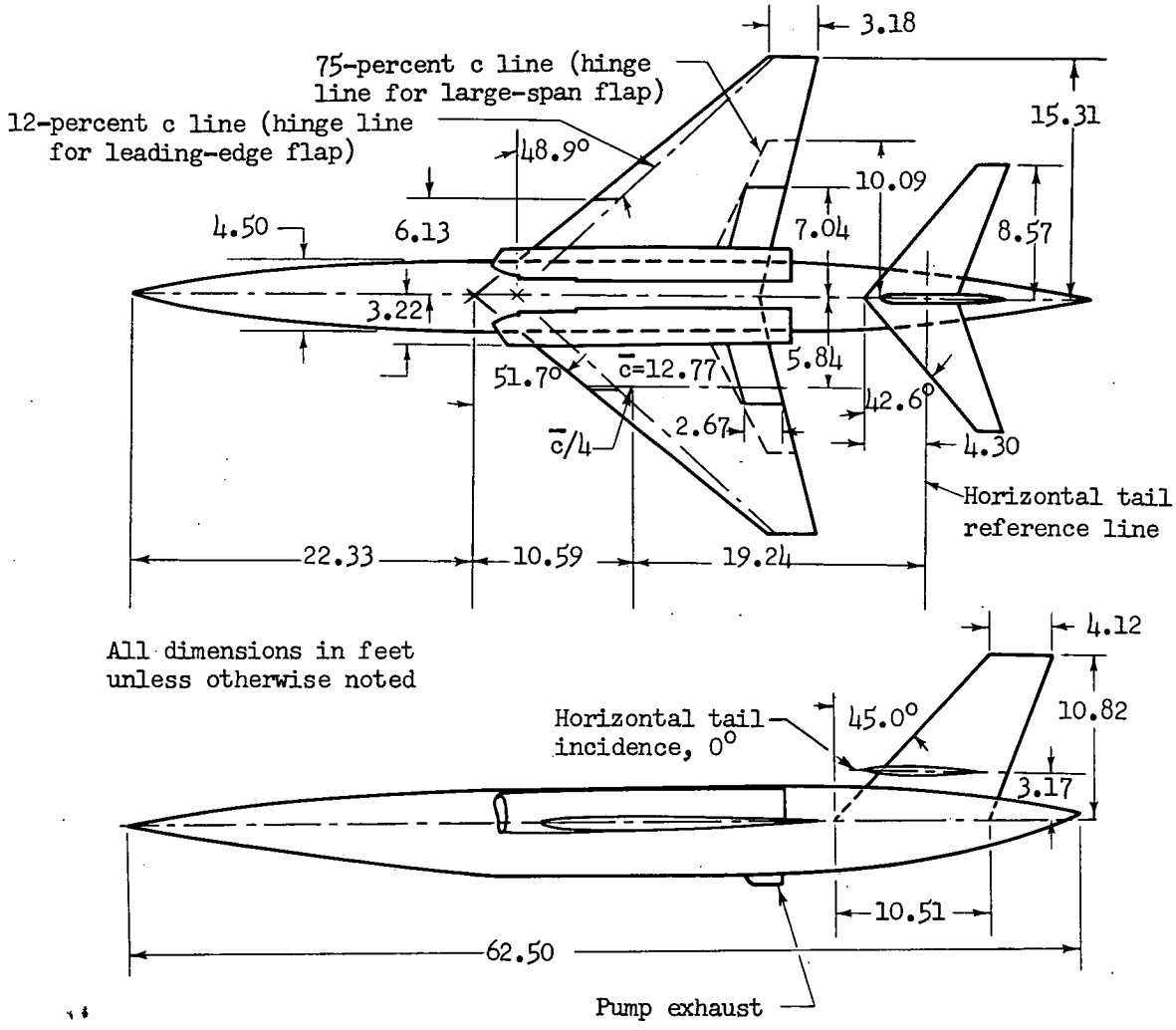

(a) Complete model.

Figure 2.- Dimensional details of the model.

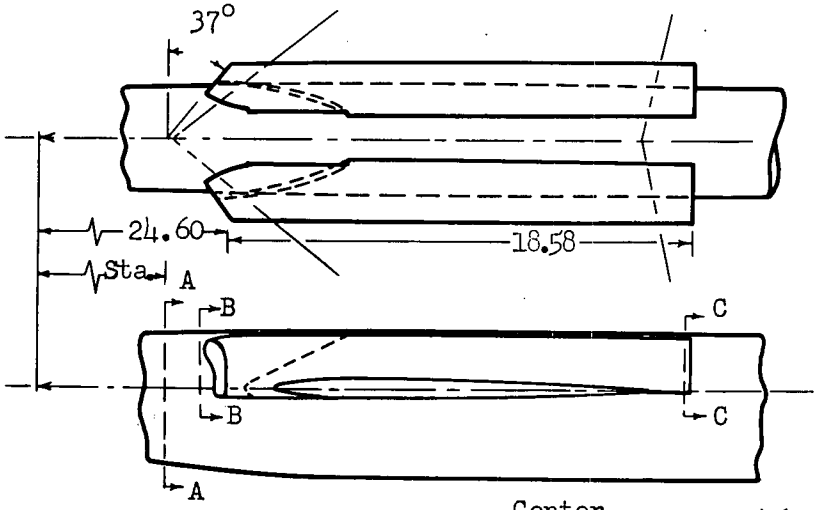

Sta.	R_1	m	H
0.70	0.23	0	0.23
1.41	.39	0	.39
4.21	.86	0	.86
8.42	1.35	0	1.35
14.04	1.81	0.23	1.81
19.65	2.09	.69	2.09
27.66	2.25	1.33	2.25
47.75	2.18	1.28	2.22
49.75	2.02	1.17	2.15
51.75	1.80	1.03	2.00
53.75	1.57	.88	1.85
55.75	1.30	.76	1.65
57.75	1.00	.64	1.40
59.75	.67	.48	1.09
61.75	.25	.20	.60

All dimensions in feet

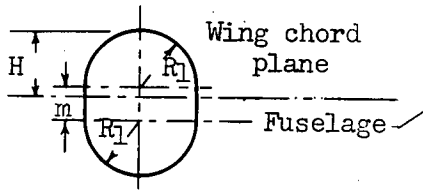

Section A-A (typical)

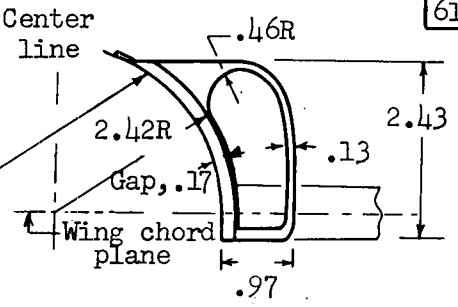

View BB-inlet area (in plane normal to free stream) 1.58 sq ft

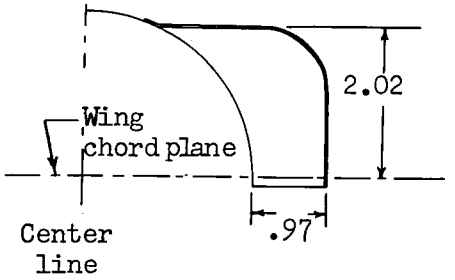

Section C-C exit area 2.52 sq ft

(b) Fuselage and external duct details.

Figure 2.- Concluded.

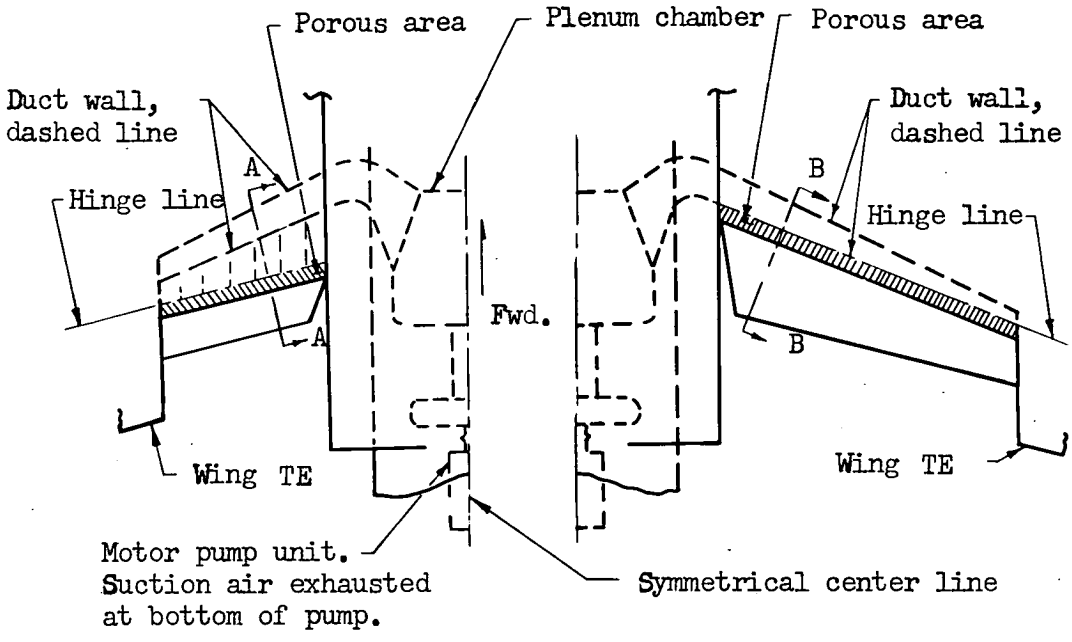

Small-span trailing-edge flap

Large-span trailing-edge flap

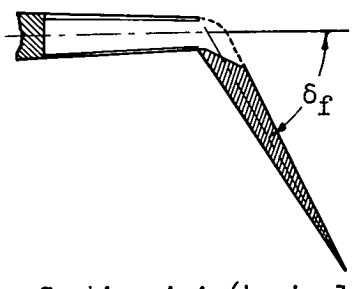

Section A-A (typical)

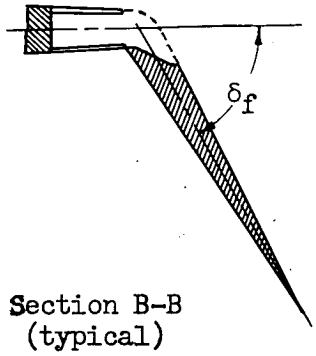

Section B-B (typical)

(a) Details of duct and pumping system.

Figure 3.- Details of porous area, duct, and pumping system.

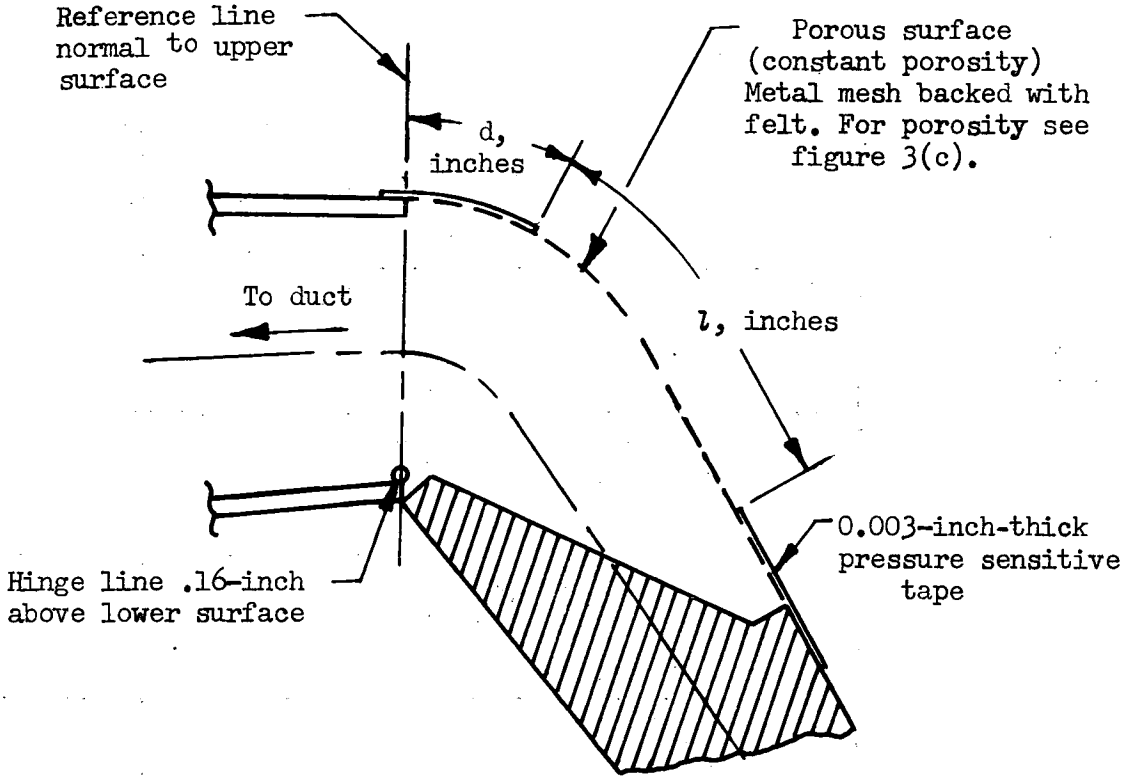

(b) Typical section of porous surface for small- and large-span trailing-edge flaps.

Figure 3.- Continued.

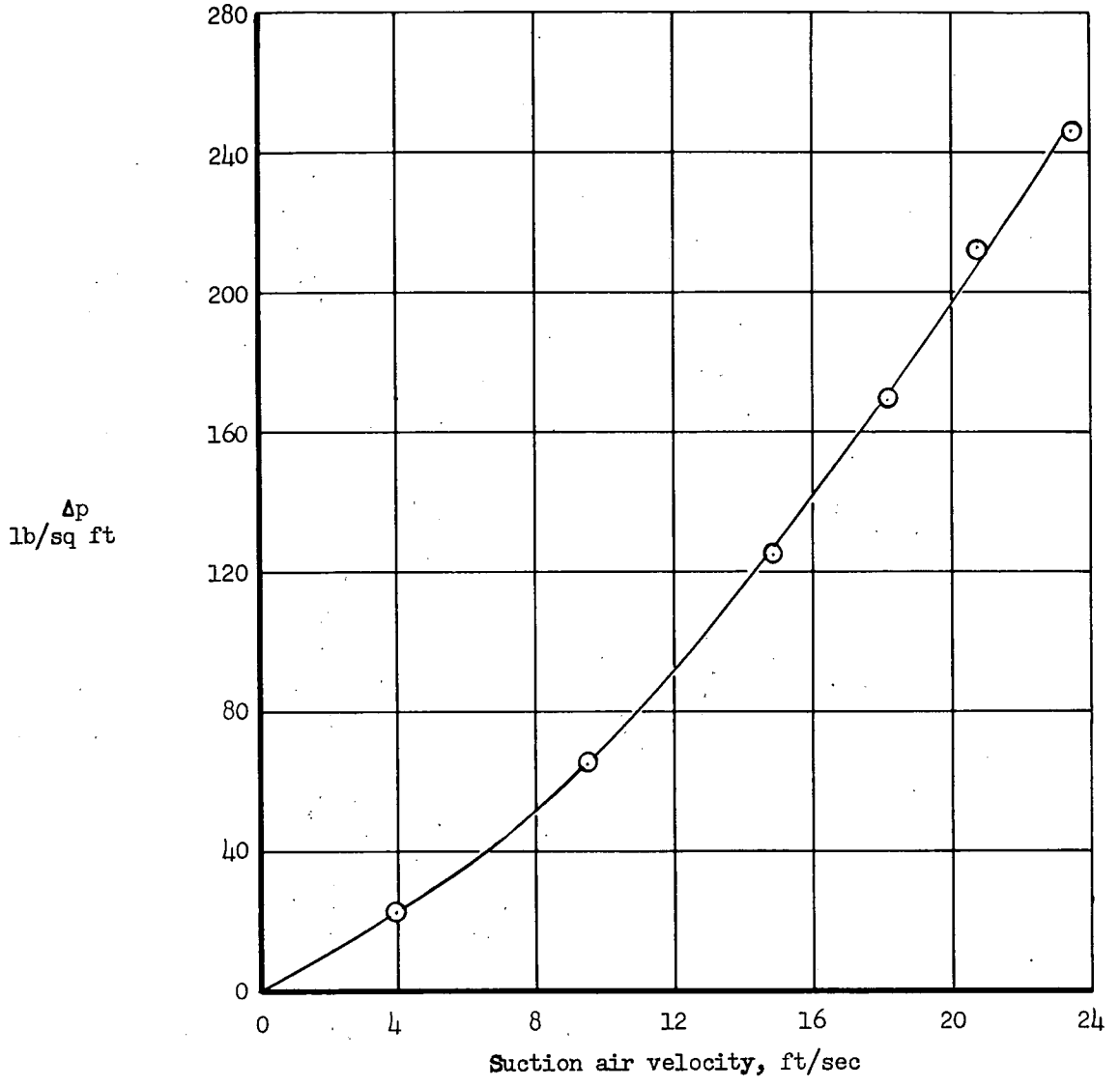

(c) Permeability of 1/16-inch felt plus metal mesh sheet used as porous surface.

Figure 3.- Concluded.

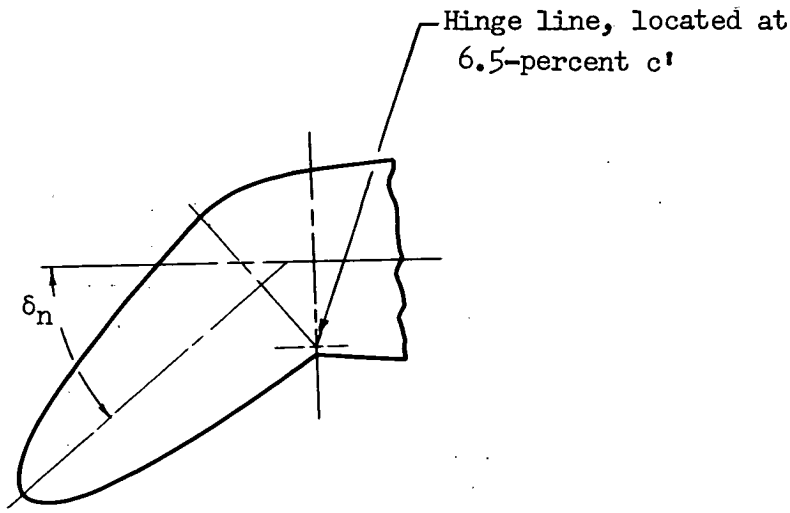

(a) Plain leading-edge flap.

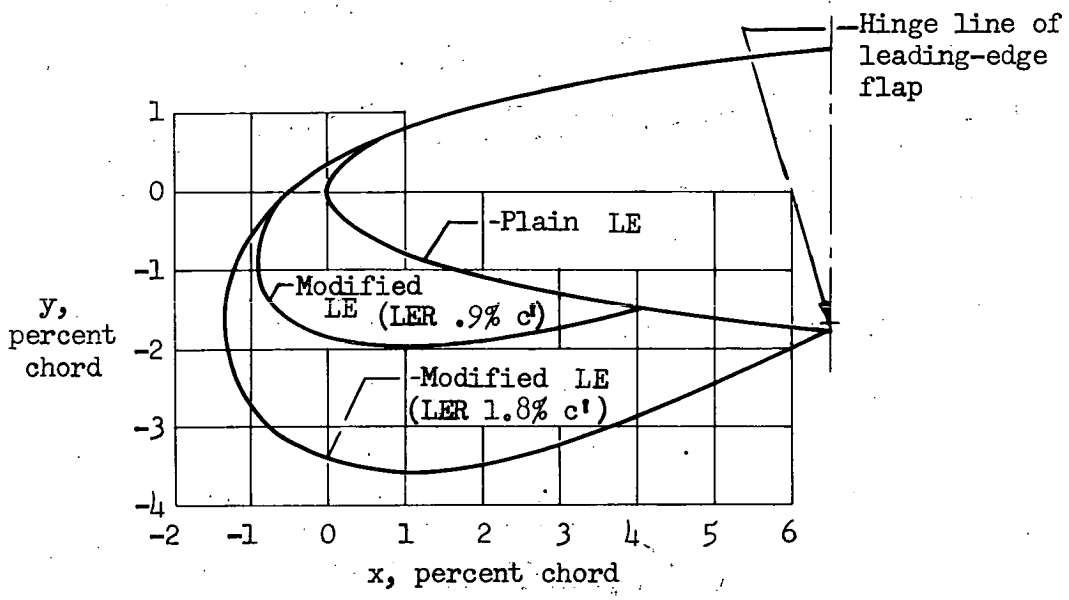

(b) Contours of the modified leading edges.

Figure 4.- Wing modifications; all sections perpendicular to the plain leading edge.

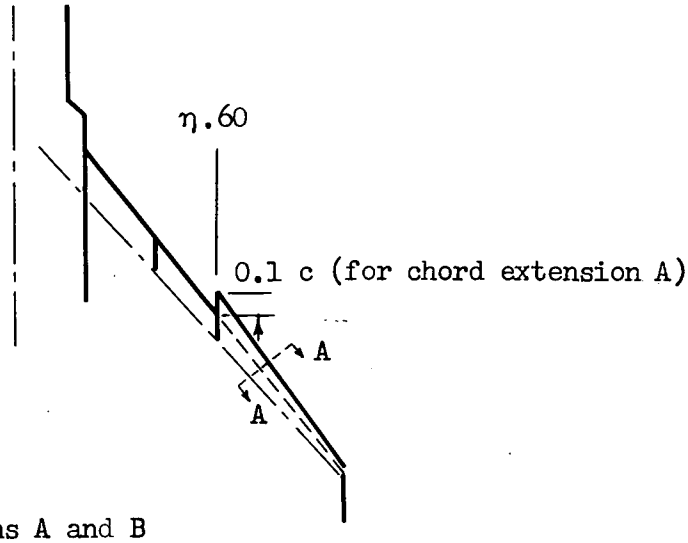

Chord extensions A and B

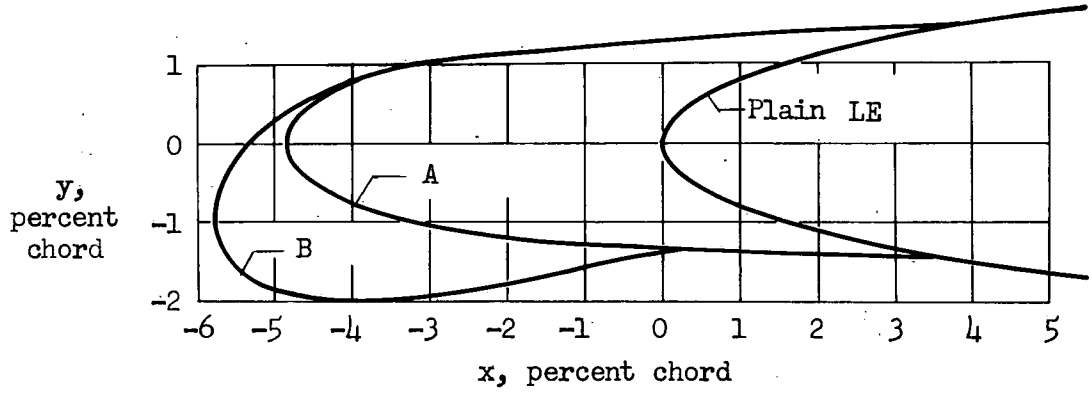

Section A-A perpendicular to plain leading edge

(c) Details of chord extensions.

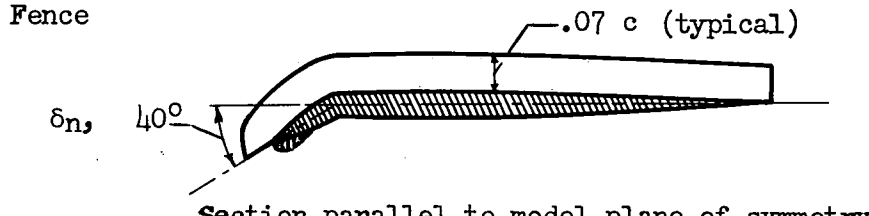

Section parallel to model plane of symmetry at $\eta = 0.70$

(d) Detail of the fence.

Figure 4.- Concluded.

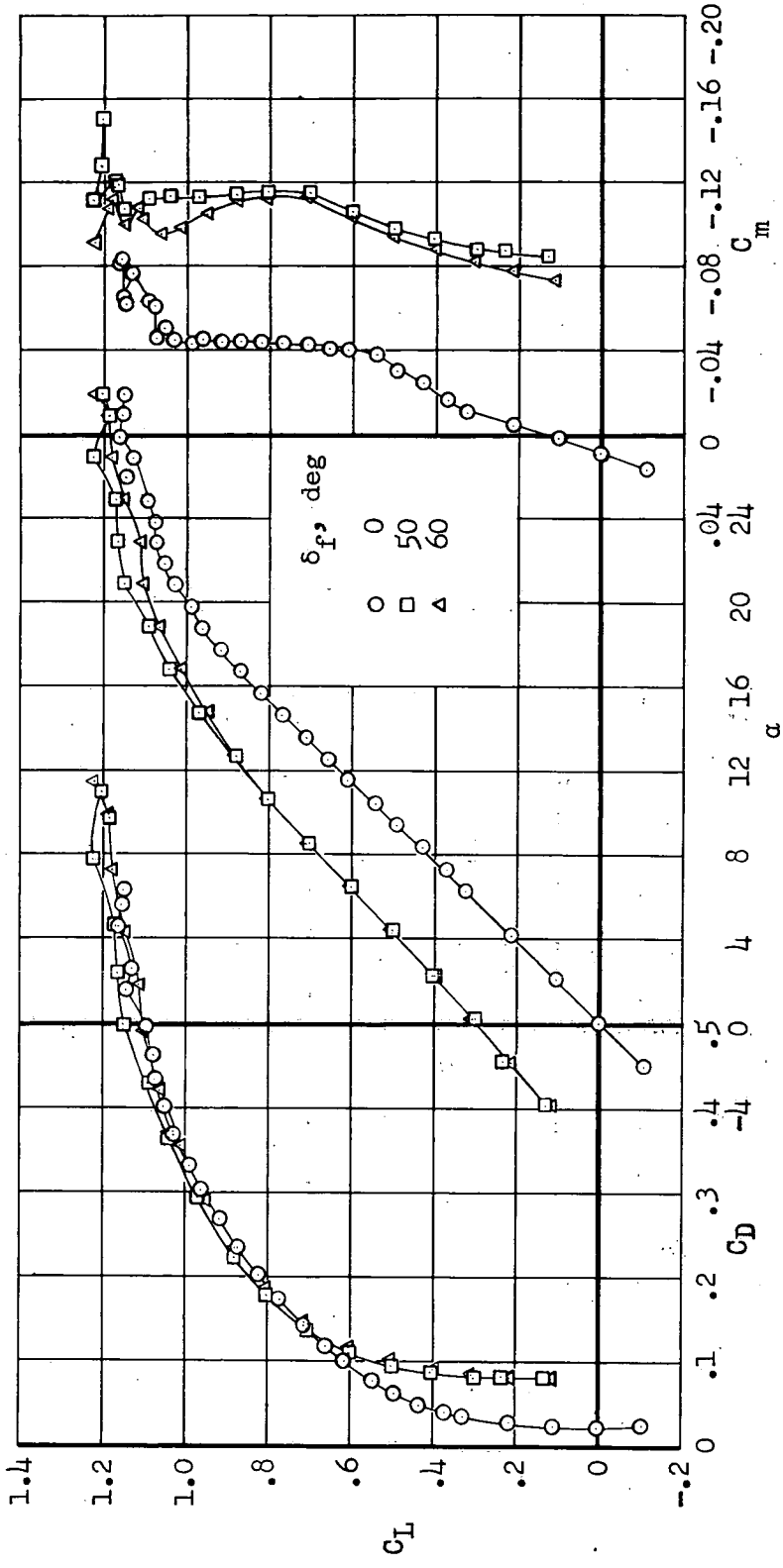

(a) Suction off.

Figure 5.- The effect of deflecting the small-span trailing-edge flap (η = 0.21 to 0.46) on the aerodynamic characteristics of the model; tail off, side-inlet duct off, plain leading edge.

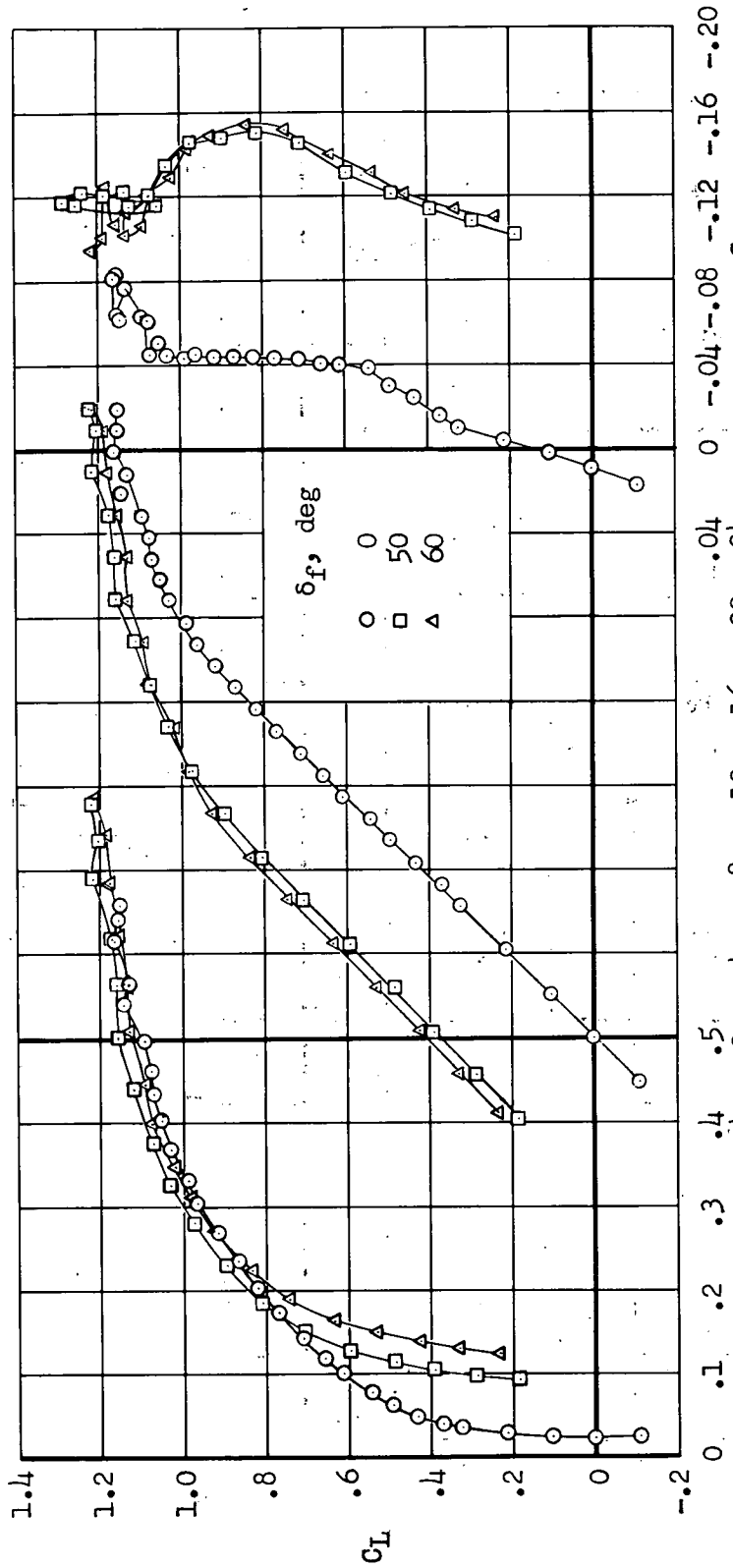

(b) Suction on.

Figure 5.- Concluded.

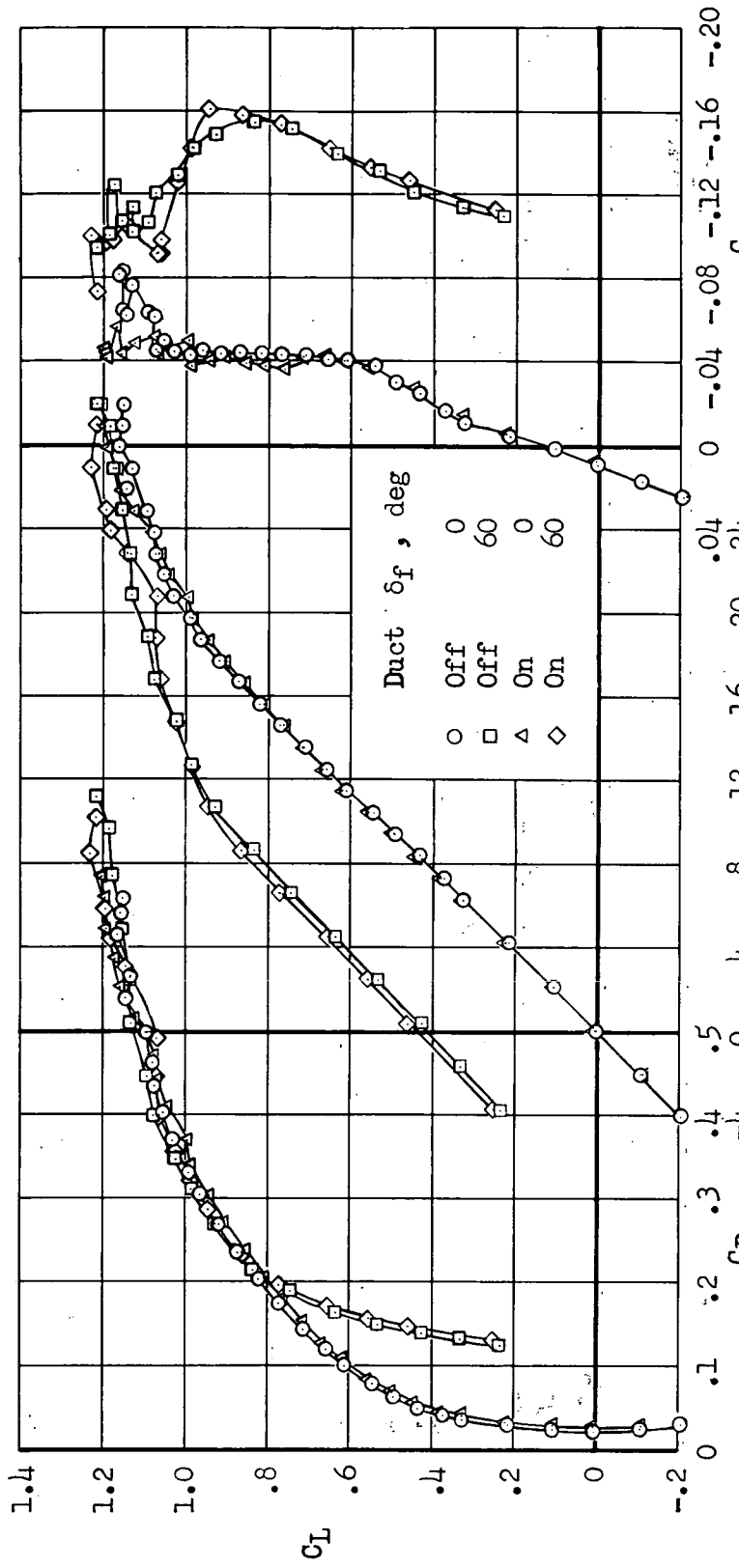

Figure 6.- The effect of the external side-inlet duct on the aerodynamic characteristics of the model with the plain leading edge; tail off, small-span trailing-edge flap (η = 0.21 to 0.46) with suction.

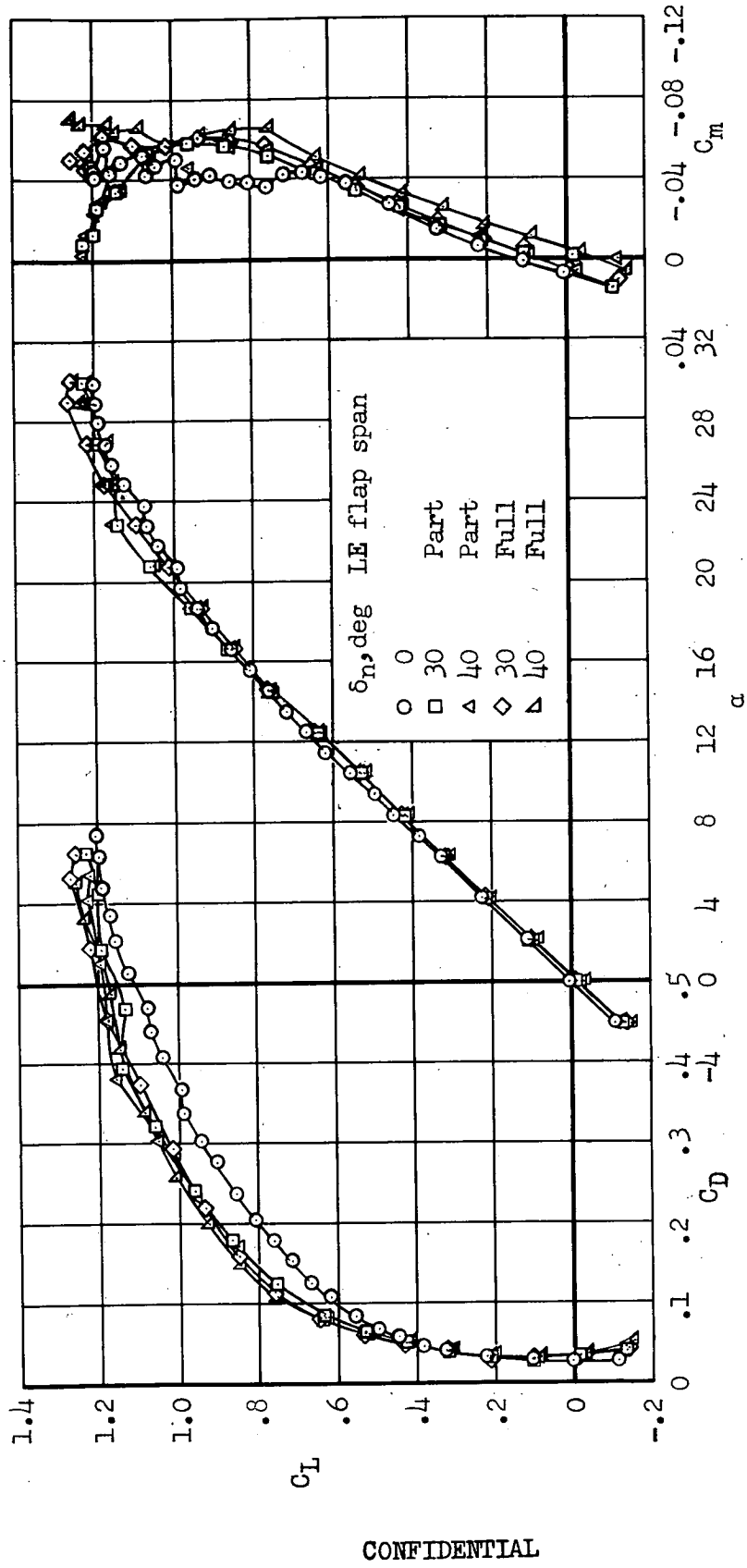

(a) Trailing-edge flap undeflected.

Figure 7.- The effect of leading-edge flap deflection on the aerodynamic characteristics of the model with plain leading edges; tail off, side-inlet duct on, small-span trailing-edge flap (η = 0.21 to 0.46). Part- and full-span leading-edge flaps extended from η = 0.40 to 1.0 and 0.21 to 1.0, respectively.

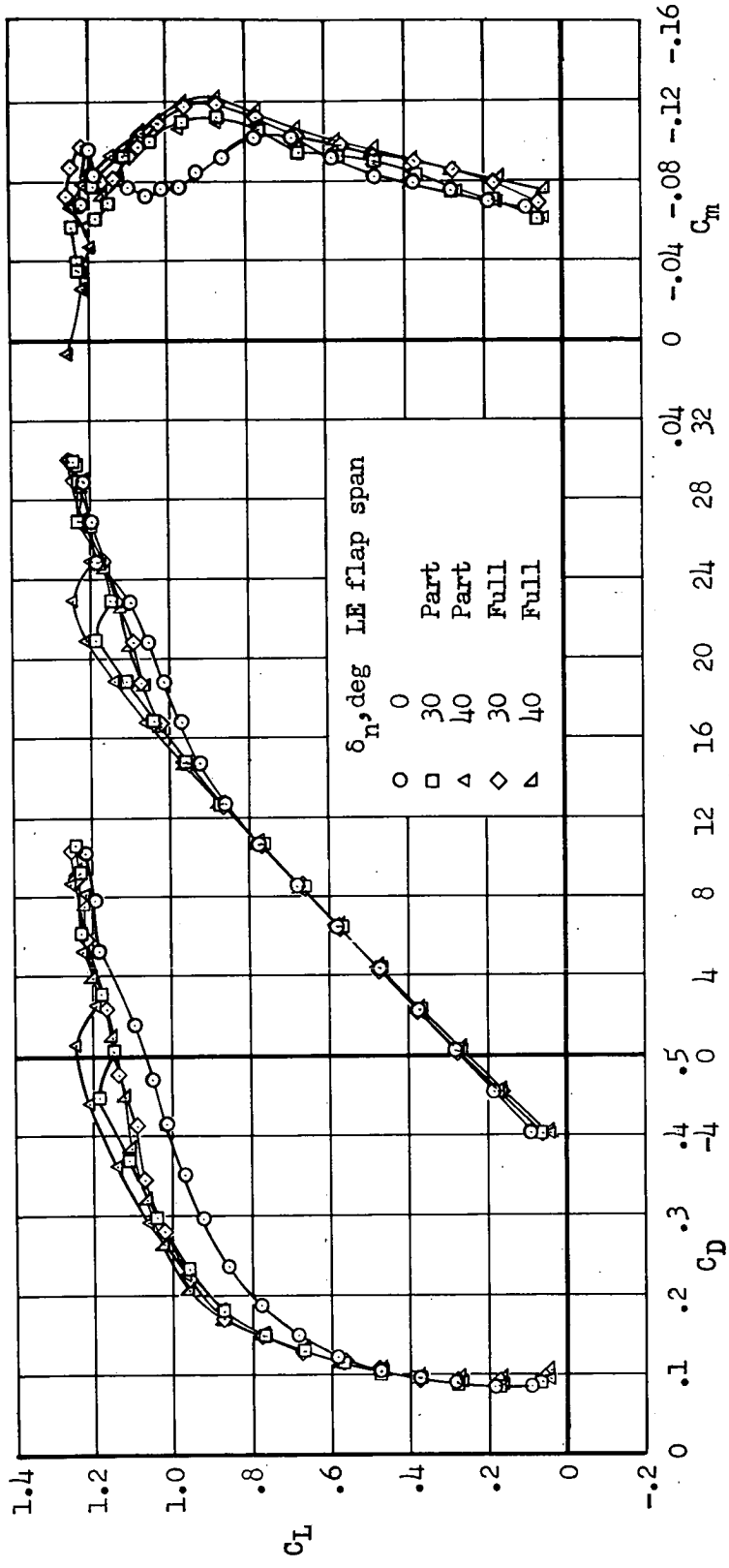

(b) Trailing-edge flap deflected 60°, suction off.

Figure 7.- Continued.

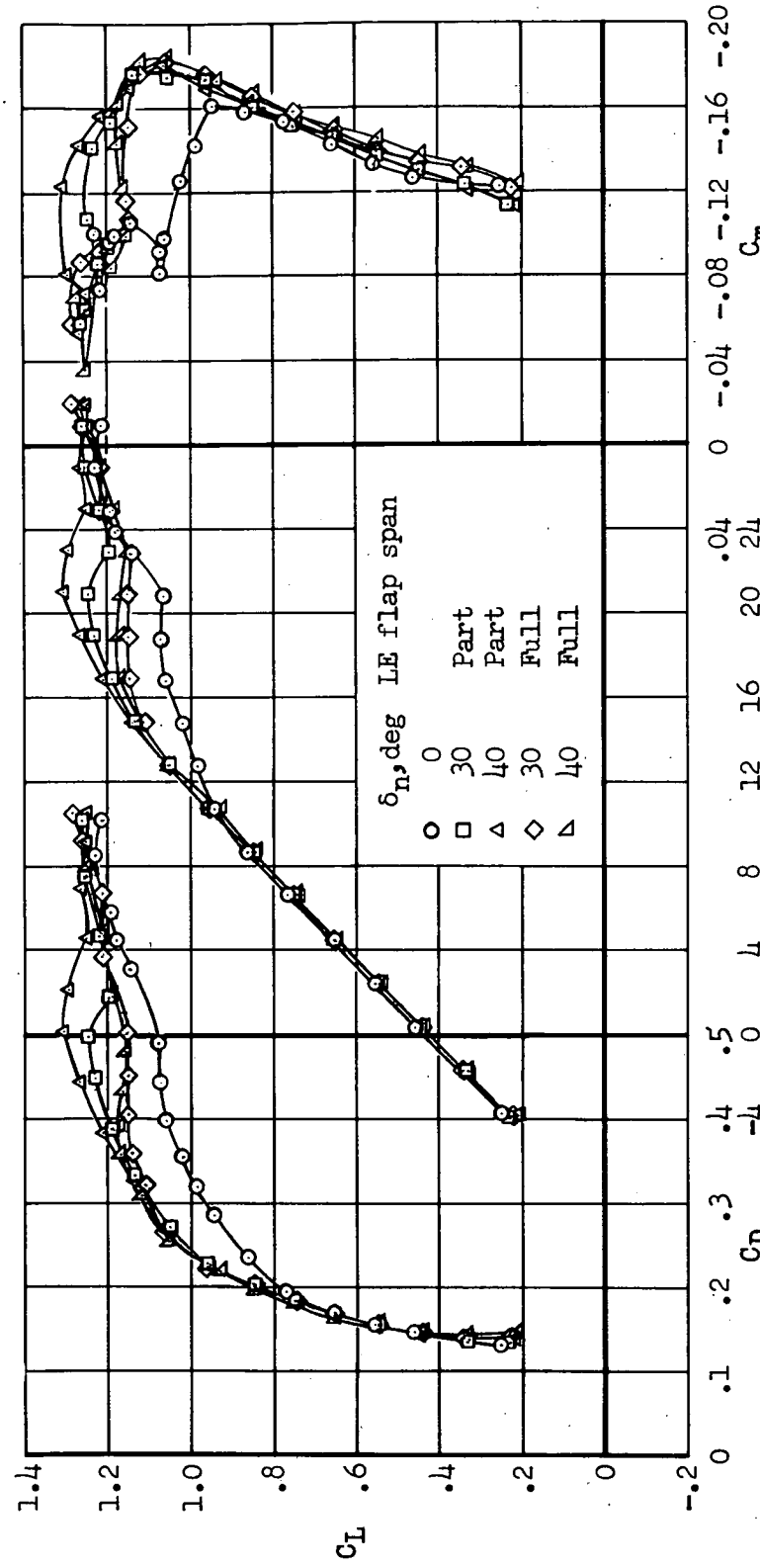

(c) Trailing-edge flap deflected 60°, suction on.

Figure 7.- Concluded.

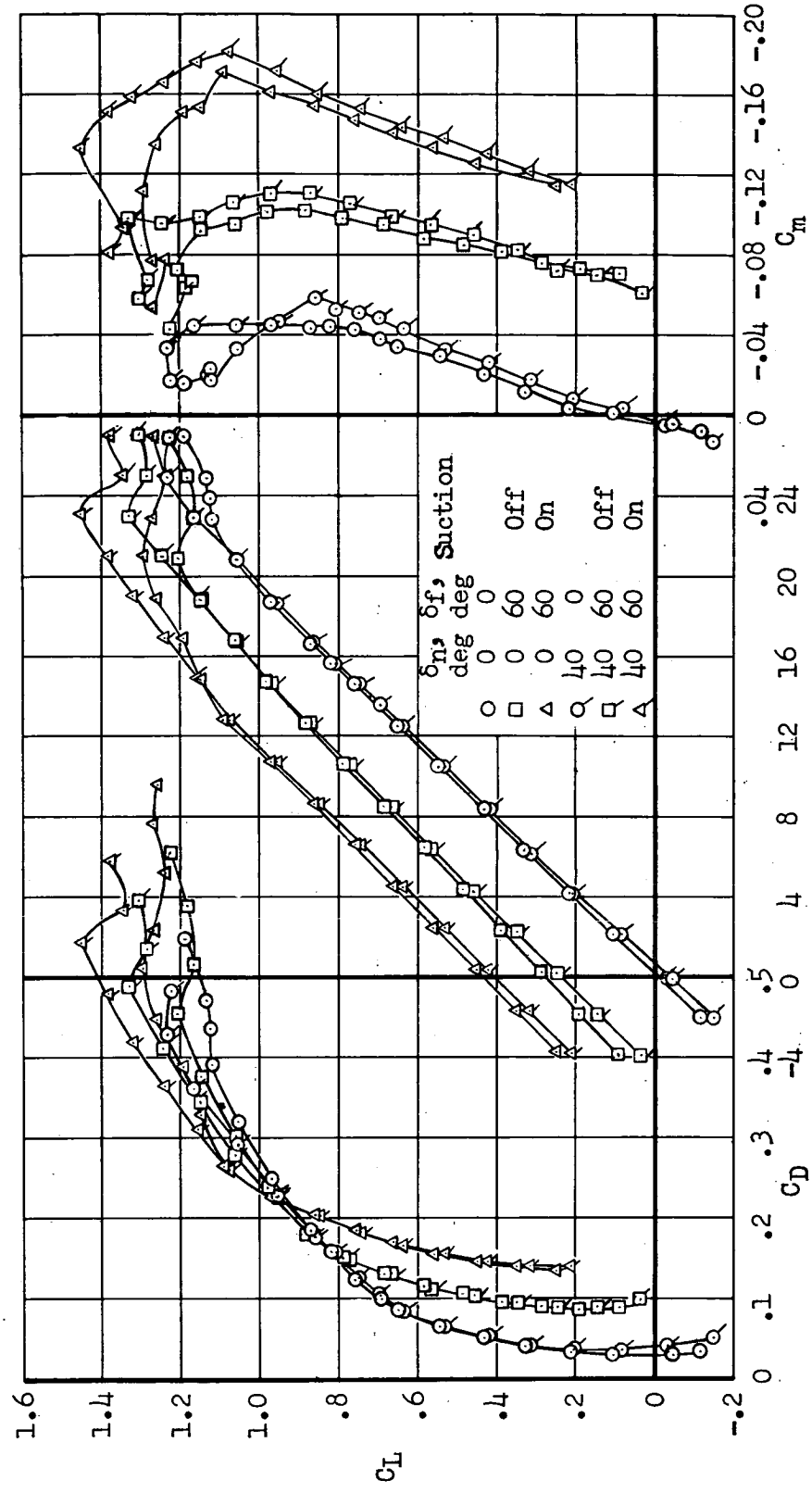

Figure 8.- The effect of trailing-edge flap deflection at two deflections of the leading-edge flap (part-span, η = 0.40 to 1.0) on the aerodynamic characteristics of the model with the modified leading edge (leading-edge radius = 1.8-percent chord); tail off, side-inlet duct on, small-span trailing-edge flap (η = 0.21 to 0.46).

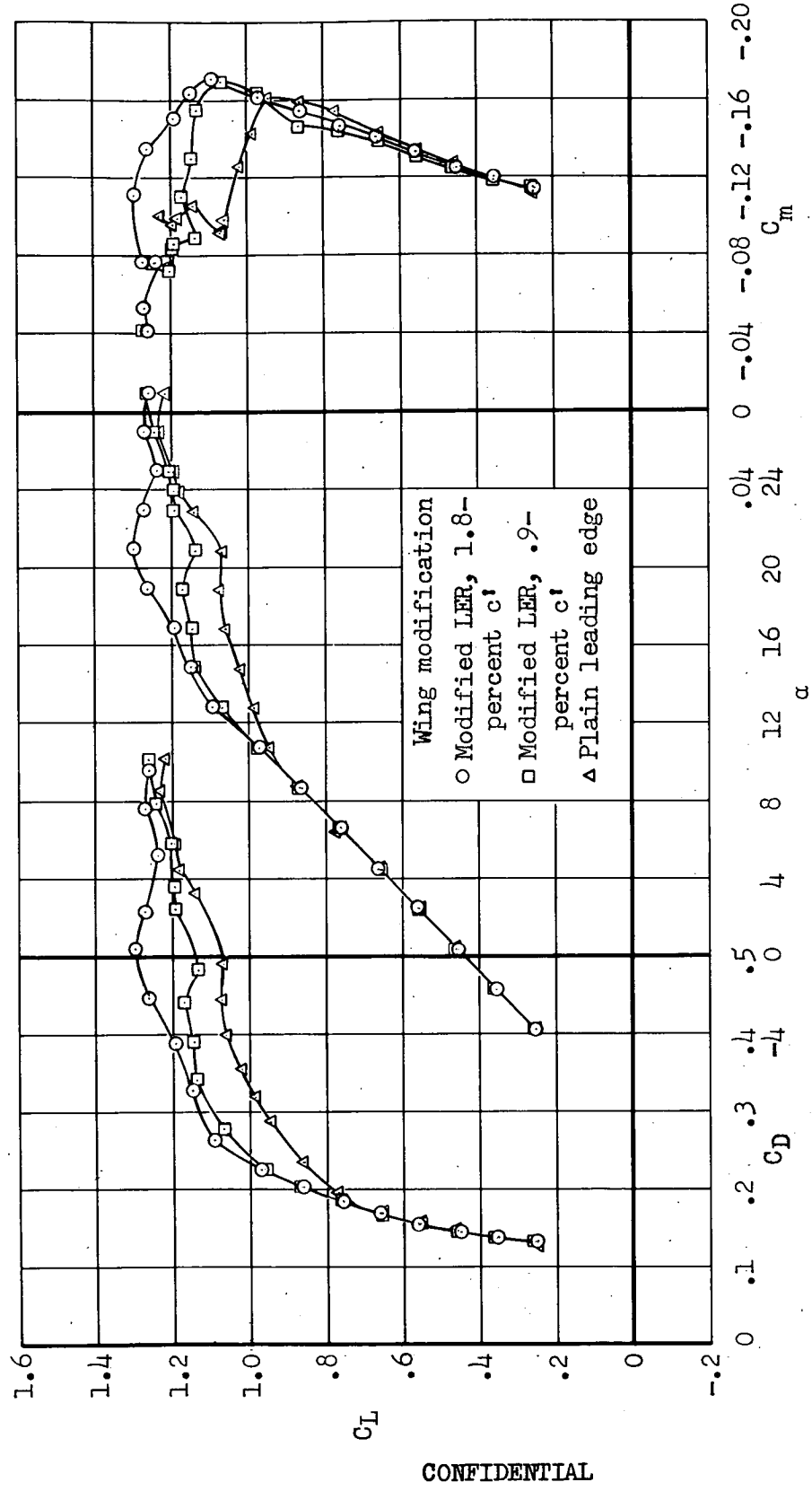

(a) $\delta_n = 0^\circ$

Figure 9.- The effect of decreasing the size of the part-span modified leading edge (η = 0.4 to 1.0) on the aerodynamic characteristics of the model with the part-span leading-edge flap (η = 0.40 to 1.0); tail off, side-inlet duct on, small-span trailing-edge flap (η = 0.21 to 0.46) deflected 60° with suction.

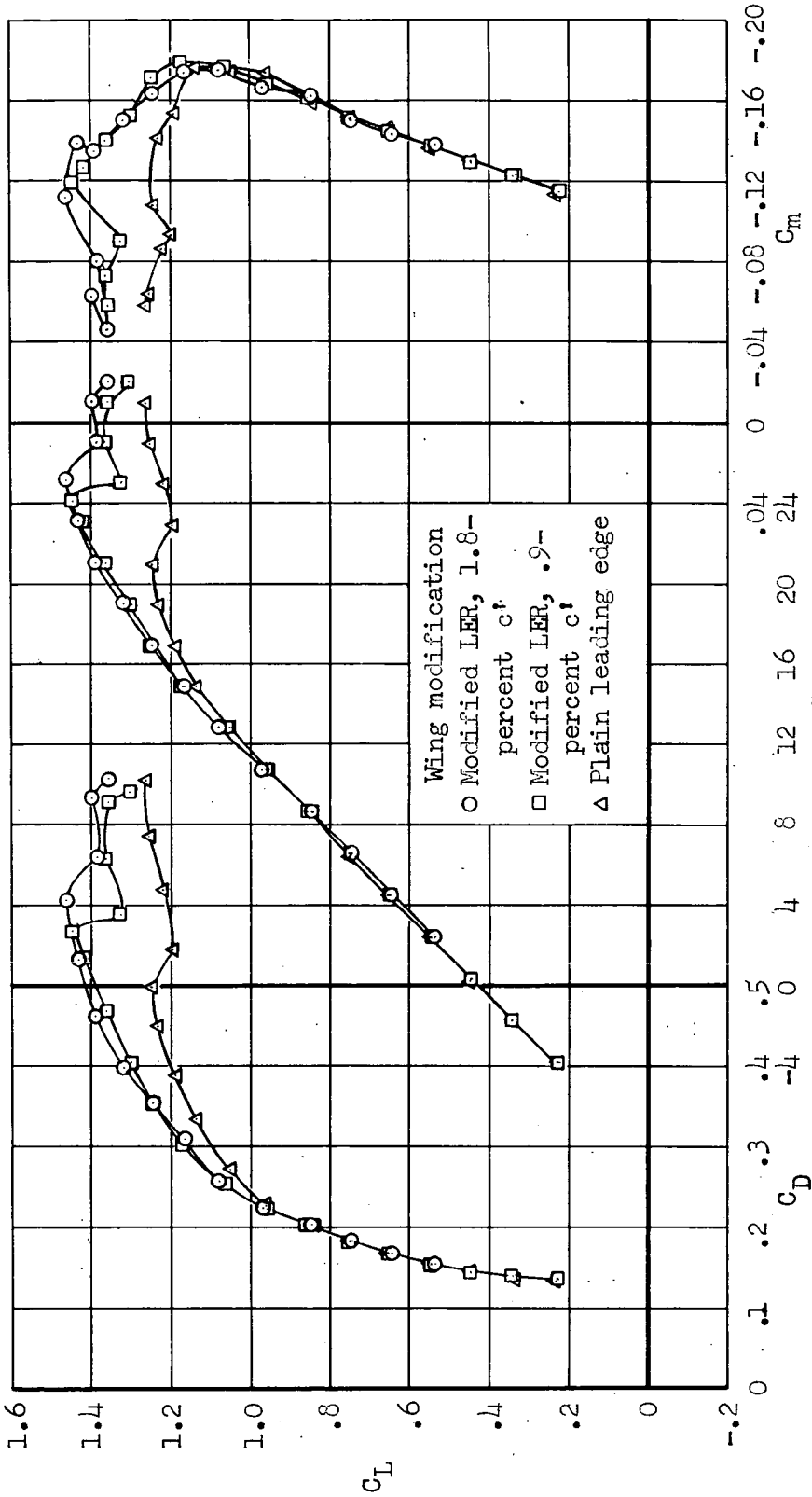

(b) $\delta_n = 30°$

Figure 9.- Concluded.

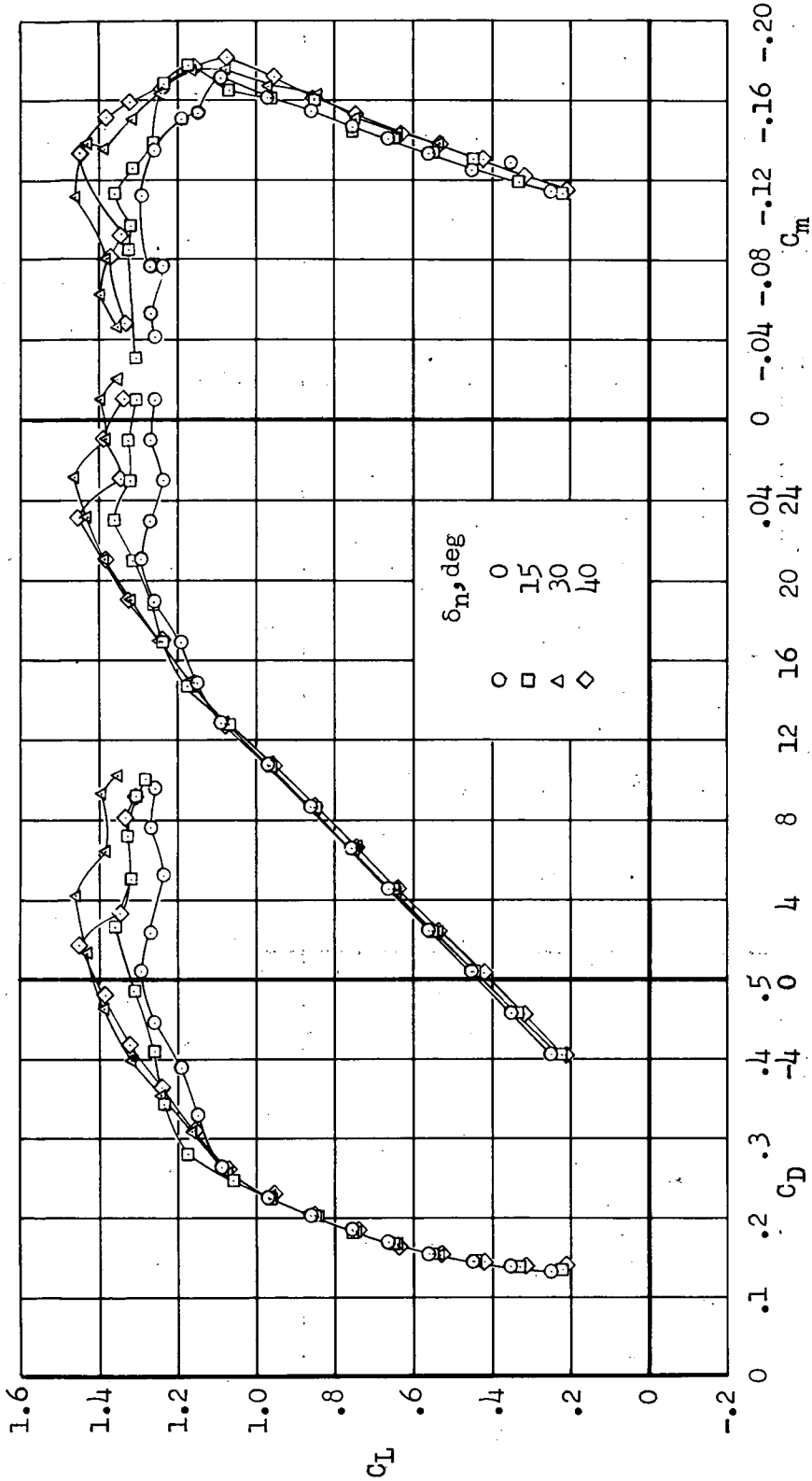

Figure 10.- The effect of part-span leading-edge flap deflection on the aerodynamic characteristics of the model with the part-span modified leading edge (leading-edge radius 1.8-percent chord, η = 0.40 to 1.0); tail off, side-inlet duct on, small-span trailing-edge flap deflected 60° with suction.

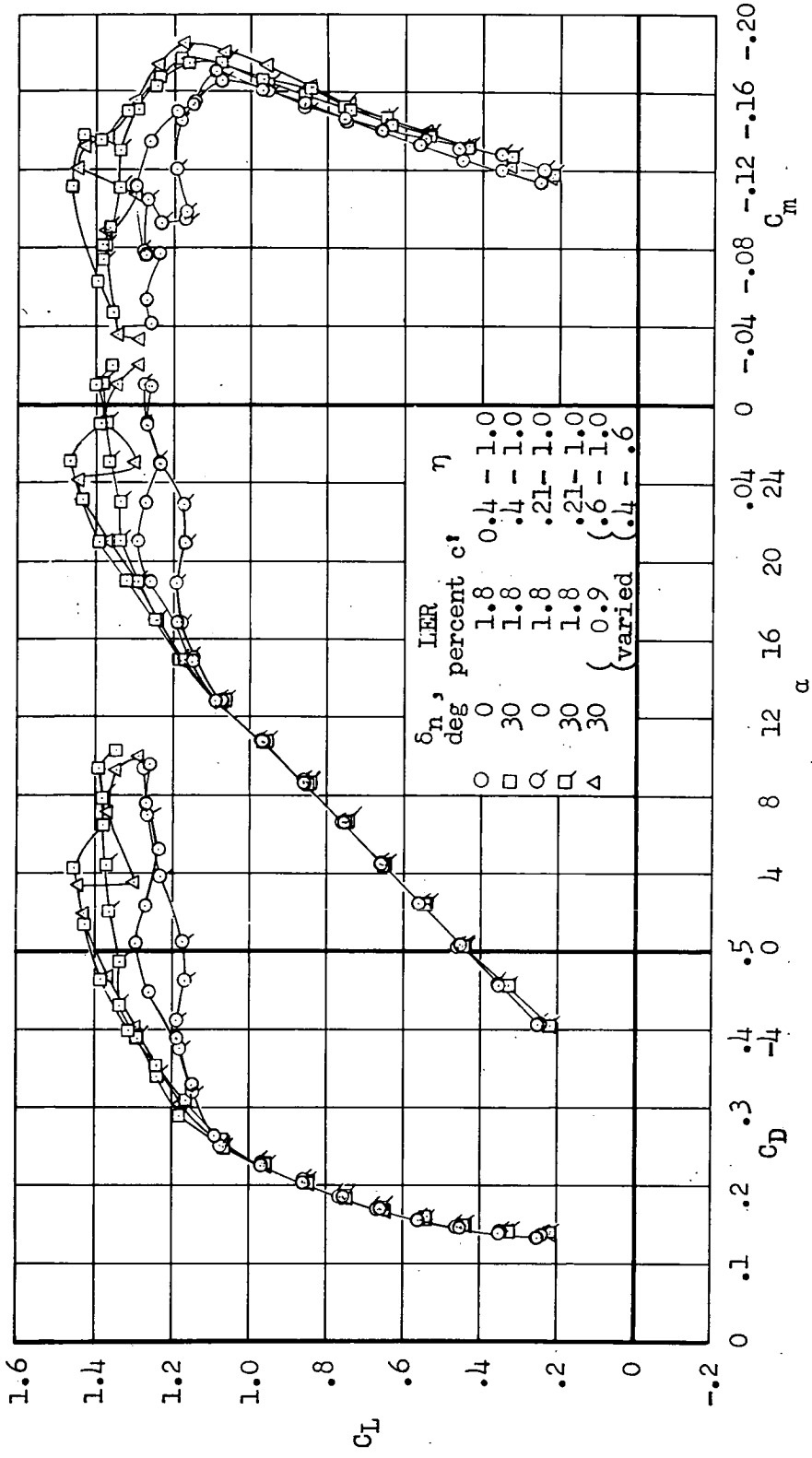

Figure 11.- The effect of several spanwise changes in the modified leading edge on the aerodynamic characteristics of the model; tail off, side-inlet duct on, small-span trailing-edge flap (η = 0.21 to 0.46) deflected 60° with suction, part-span leading-edge flap (η = 0.40 to 1.0).

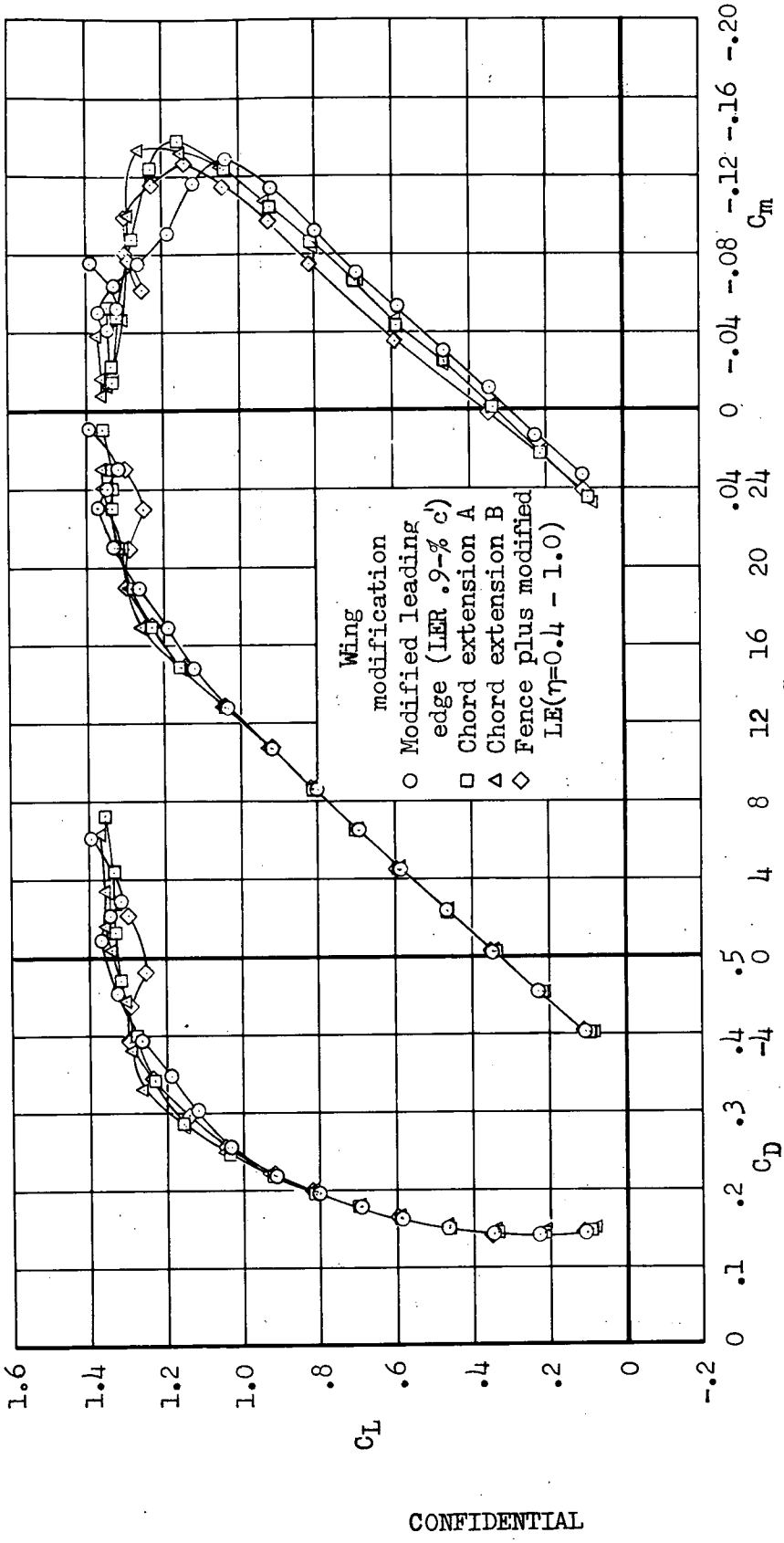

(a) Tail dihedral angle, $\Gamma = 0^\circ$.

Figure 12.- The effect of chord extension and fence configurations on the tail-on aerodynamic characteristics of the model; side-inlet duct on, small-span trailing-edge flap (η = 0.21 to 0.46) deflected 60° with suction, part-span leading-edge flap (η = 0.40 to 1.0) deflected 40°.

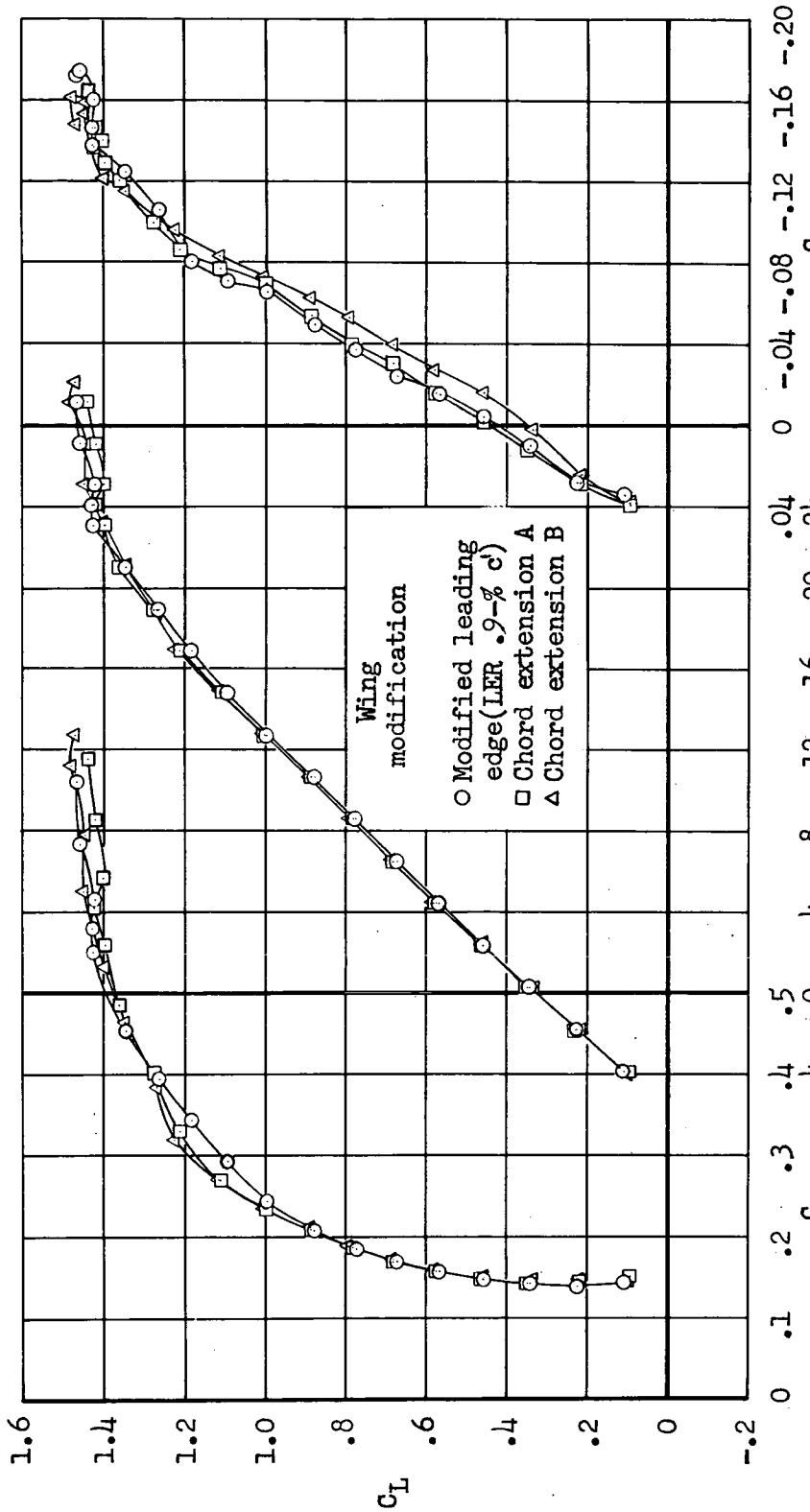

(b) Tail dihedral angle, Γ = -25°.

Figure 12.- Concluded.

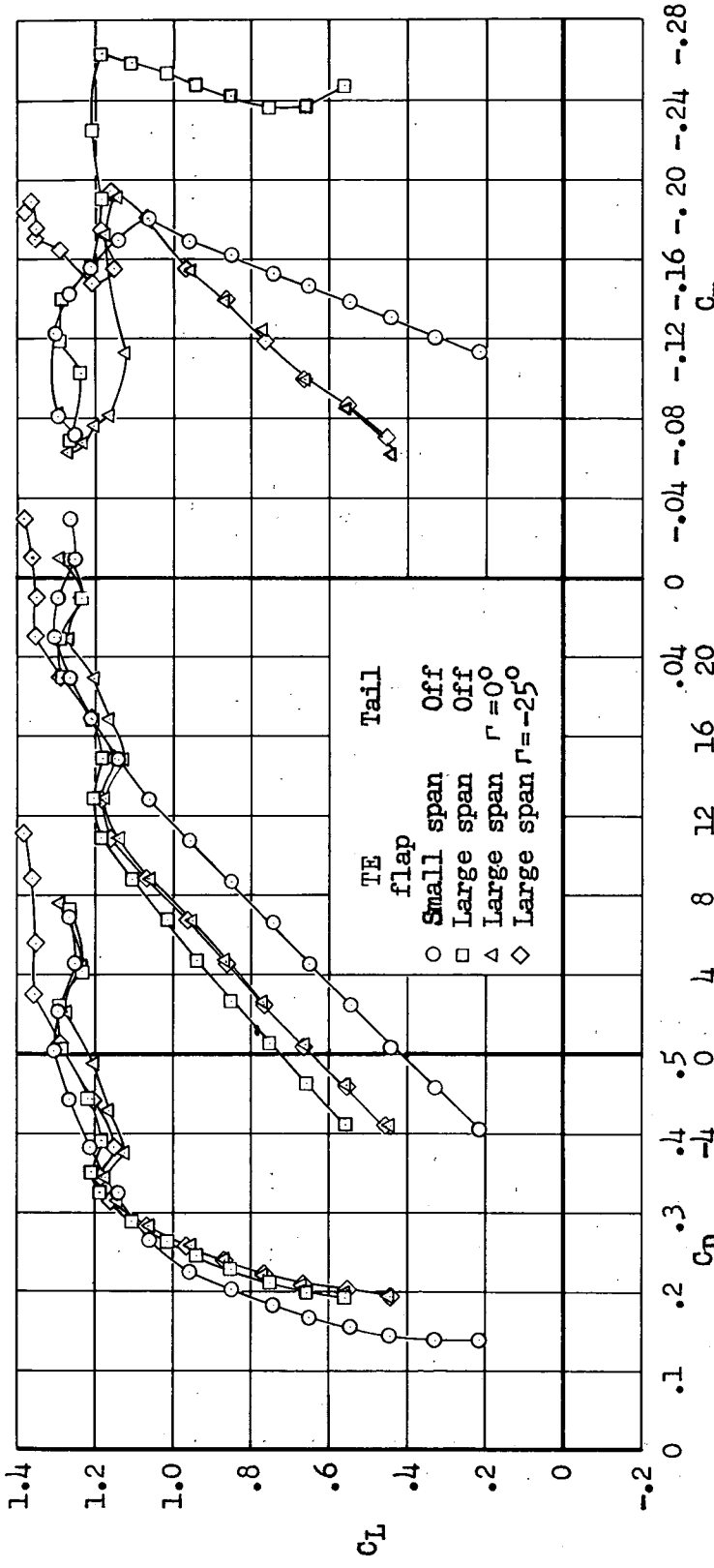

Figure 13.- The effect of the large-span trailing-edge flap (η = 0.21 to 0.66) deflected 60° with suction on the aerodynamic characteristics of the model; side-inlet duct on, plain leading edge, part-span leading-edge flap (η = 0.40 to 1.0) deflected 40°.

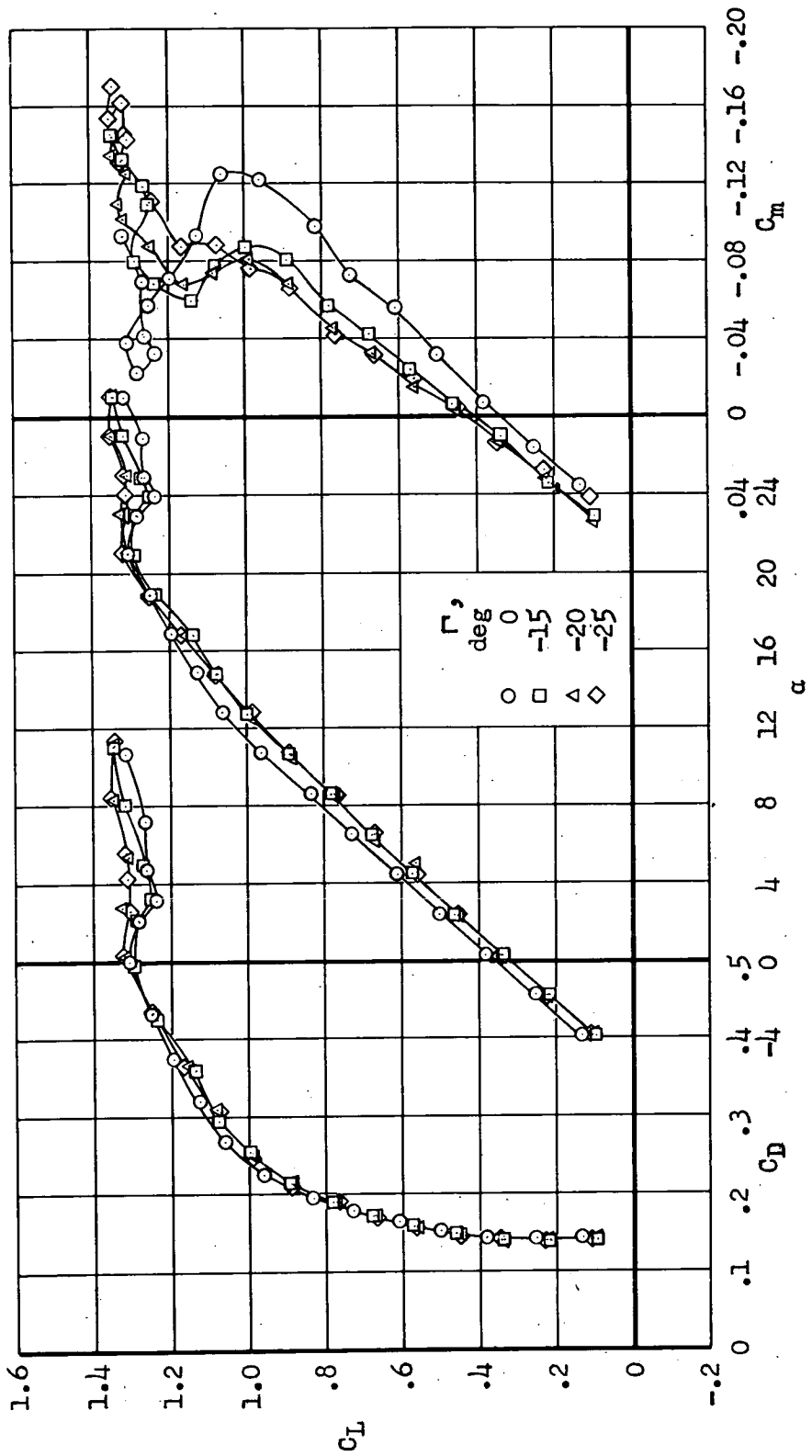

Figure 14.- The effect of horizontal-tail droop on the aerodynamic characteristics of the model with the plain leading edge and the part-span leading-edge flap (η = 0.40 to 1.0) deflected 40°; side-inlet duct on, small-span trailing-edge flap (η = 0.21 to 0.46) deflected 60° with suction.

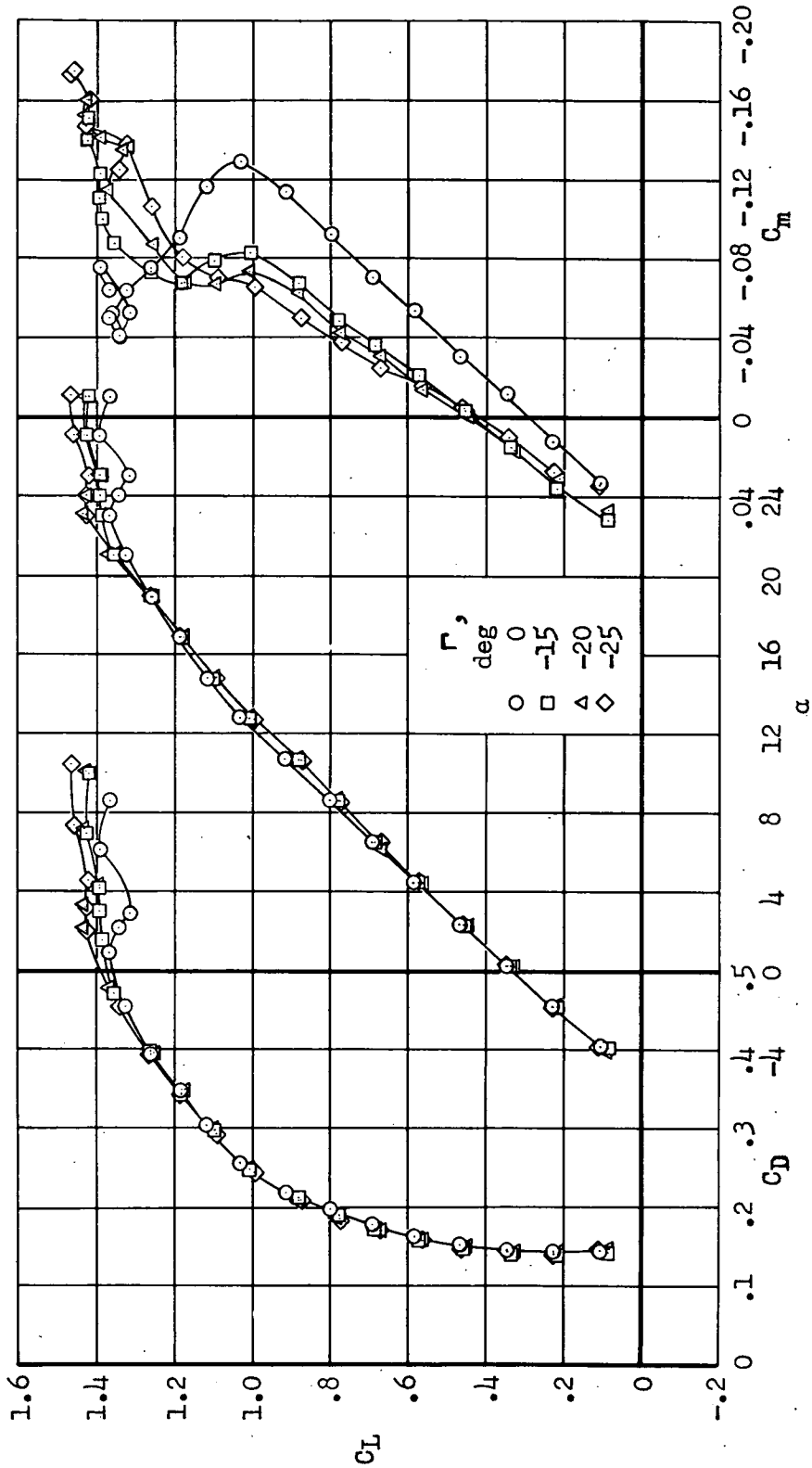

Figure 15.- The effect of horizontal-tail droop on the aerodynamic characteristics of the model with the modified leading edge (leading-edge radius of 0.9-percent chord, η = 0.40 to 1.0) on the part-span leading-edge flap (η = 0.40 to 1.0) deflected 40°; side-inlet duct on, small-span trailing-edge flap (η = 0.21 to 0.46) deflected 60° with suction.

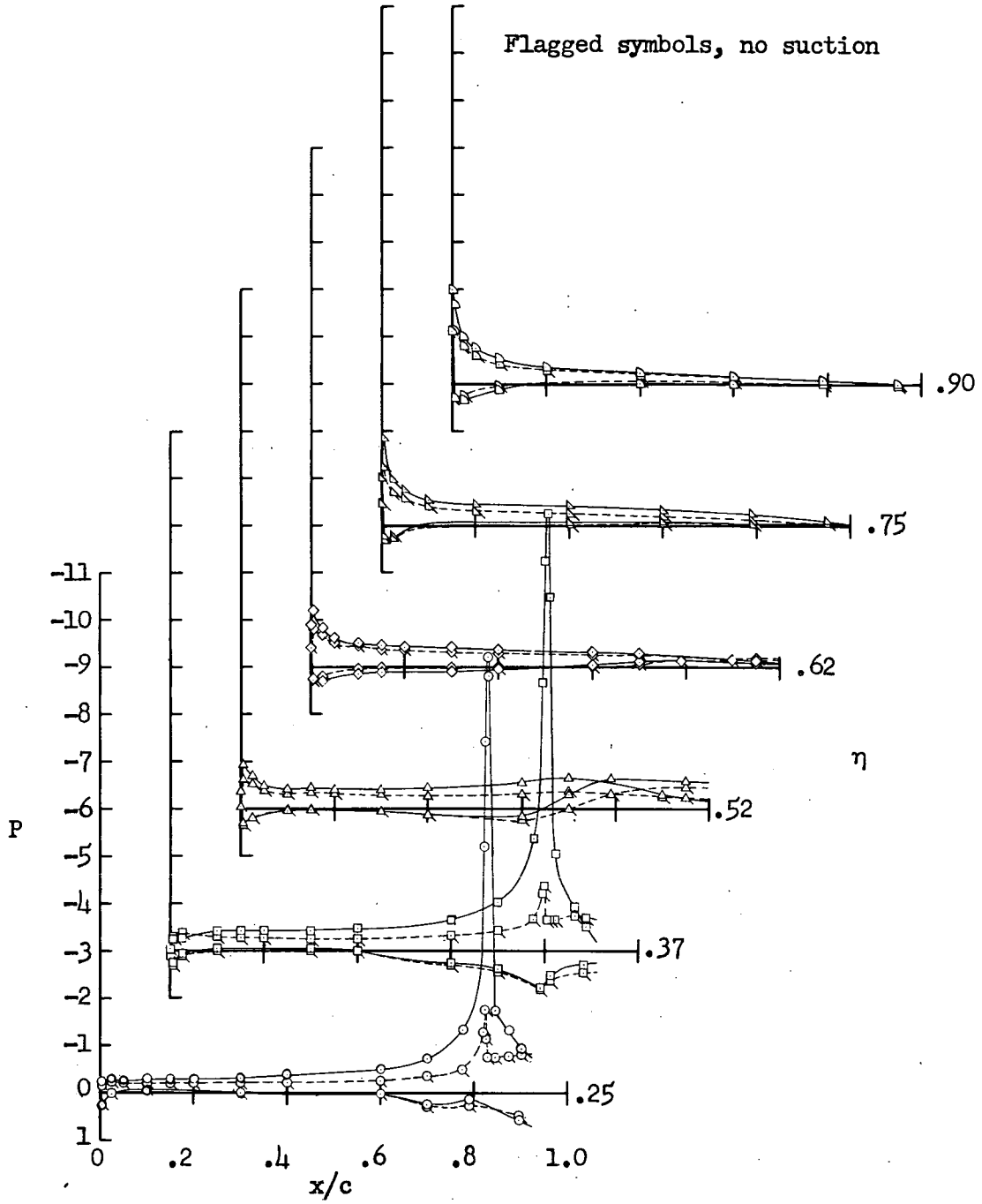

(a) $\alpha = 0.2^{\circ}$

Figure 16.- Chordwise pressure distributions on the wing with leading-edge flap undeflected and with the small-span trailing-edge flap (η = 0.21 to 0.46) deflected 60° with and without suction; side-inlet duct on.

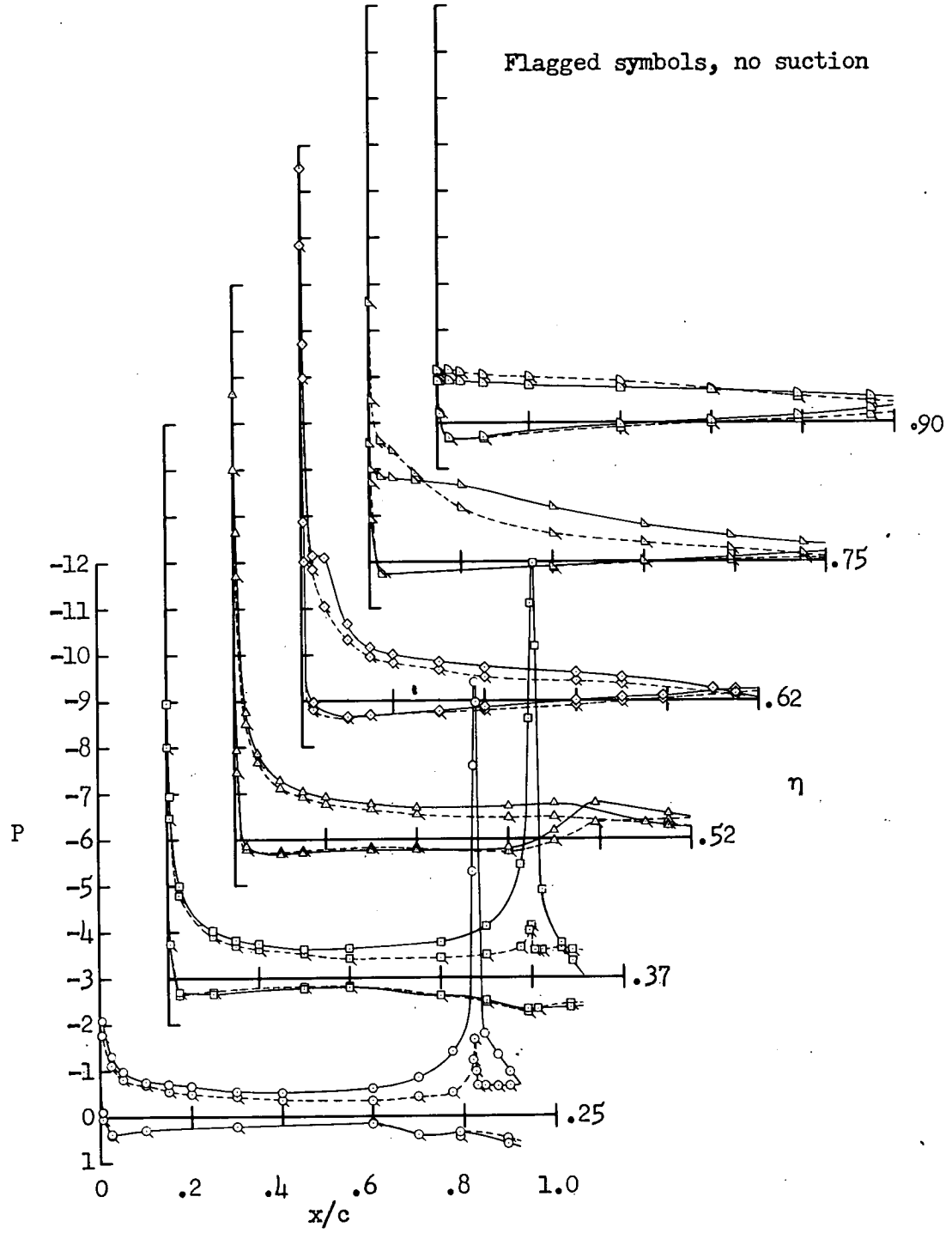

(b) $\alpha = 8.7^\circ$

Figure 16.- Continued.

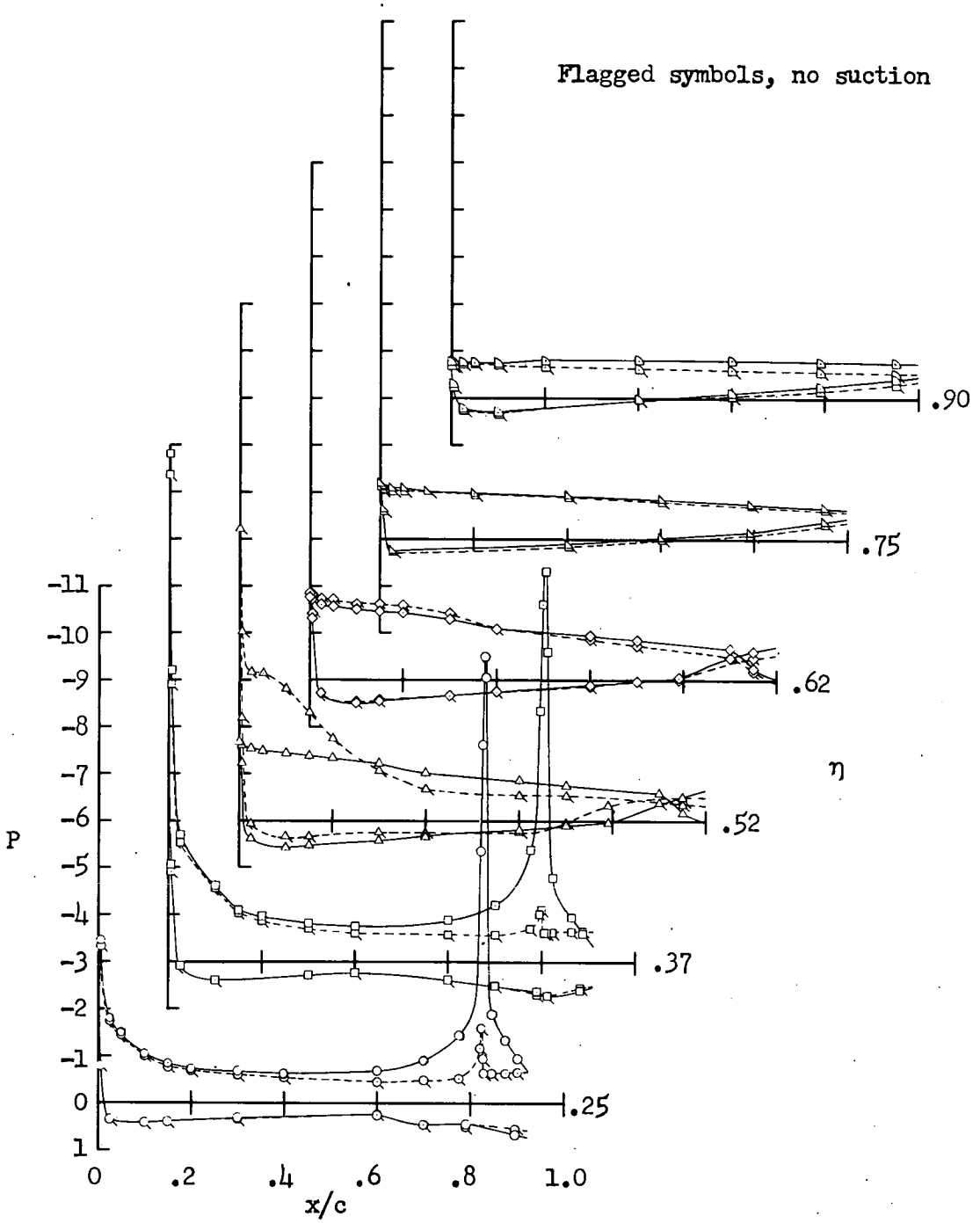

(c) $\alpha = 12.8^{\circ}$

Figure 16.- Continued.

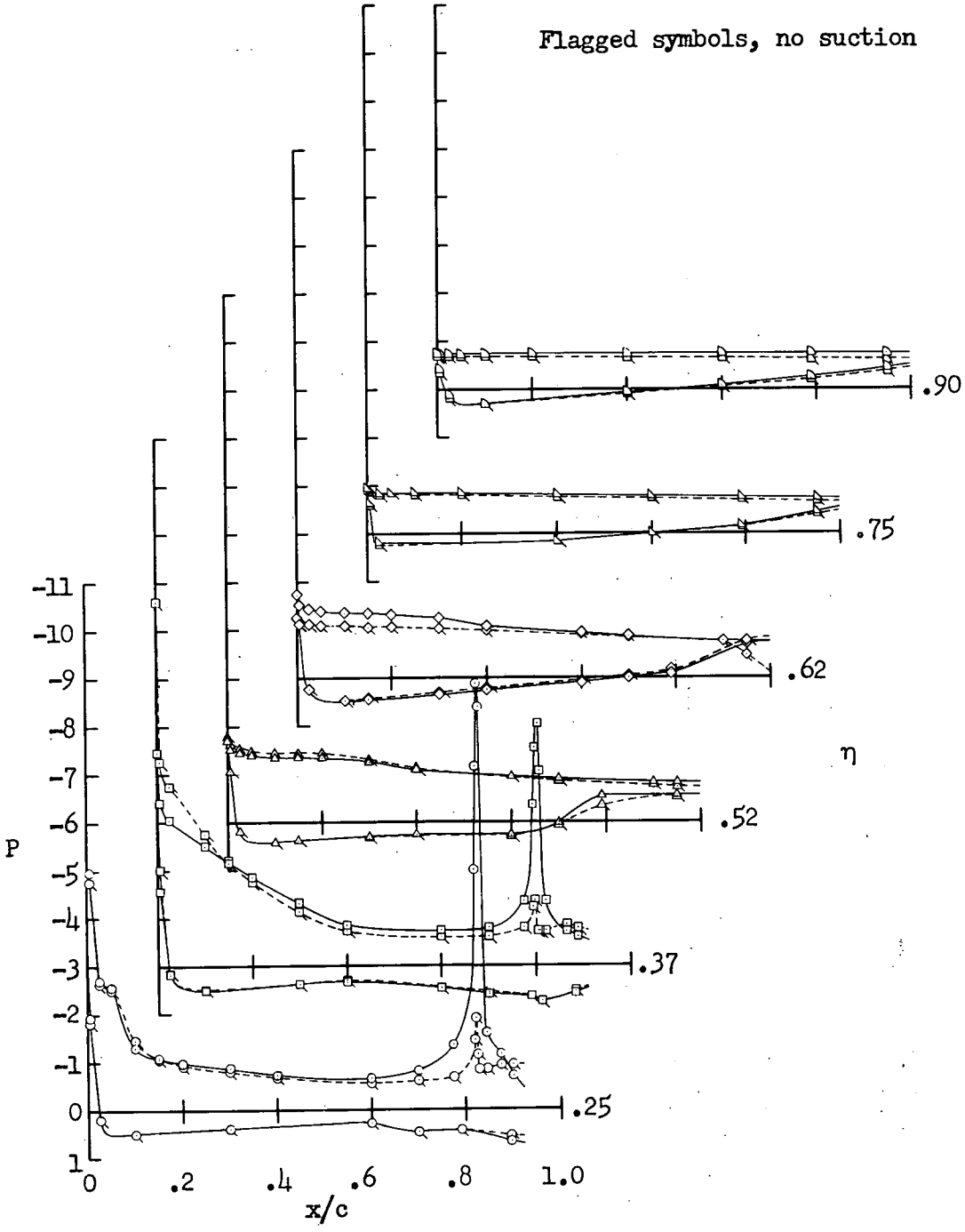

(d) $\alpha = 16.8^{\circ}$

Figure 16.- Continued.

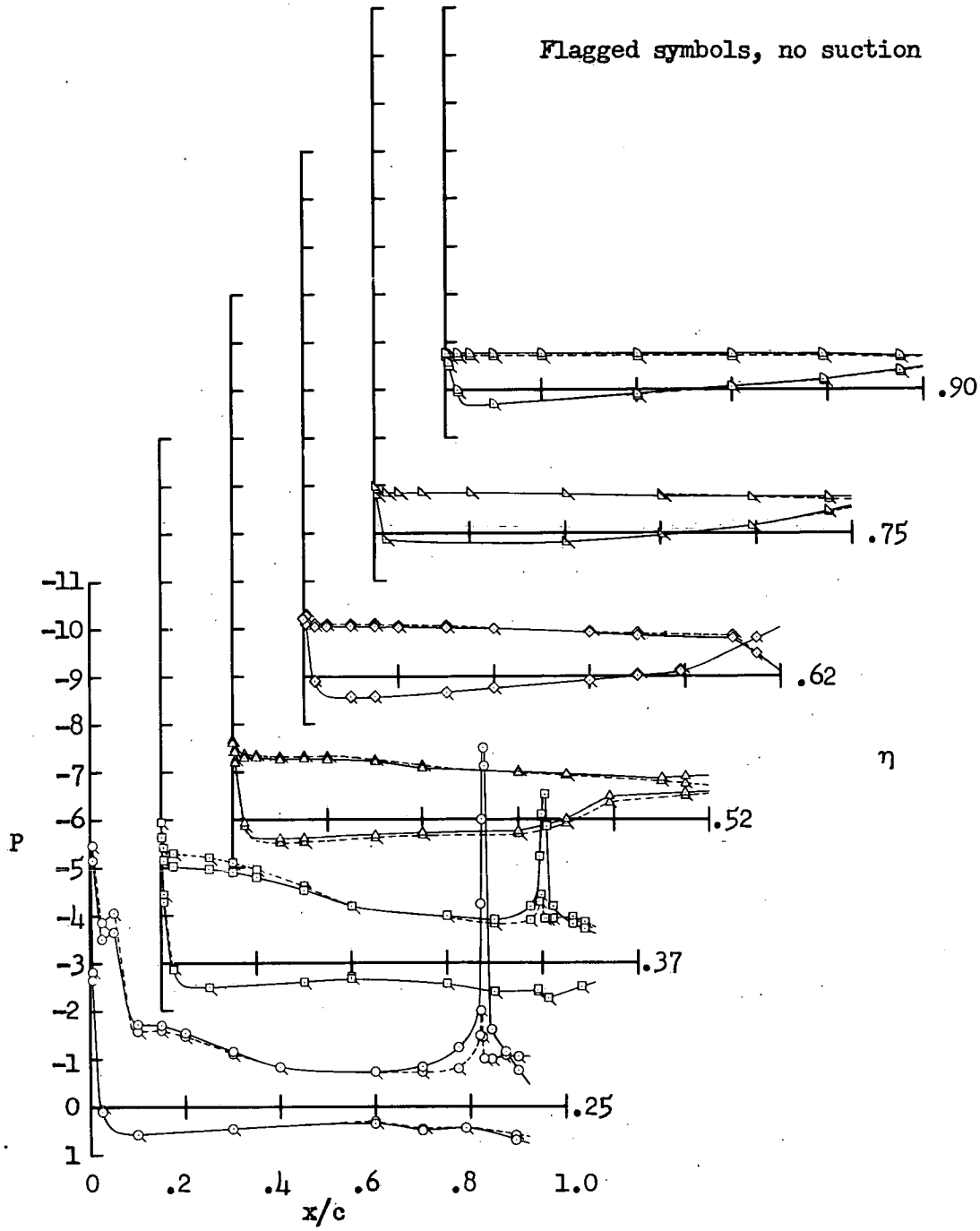

(e) $\alpha = 20.8^{\circ}$

Figure 16.- Concluded.

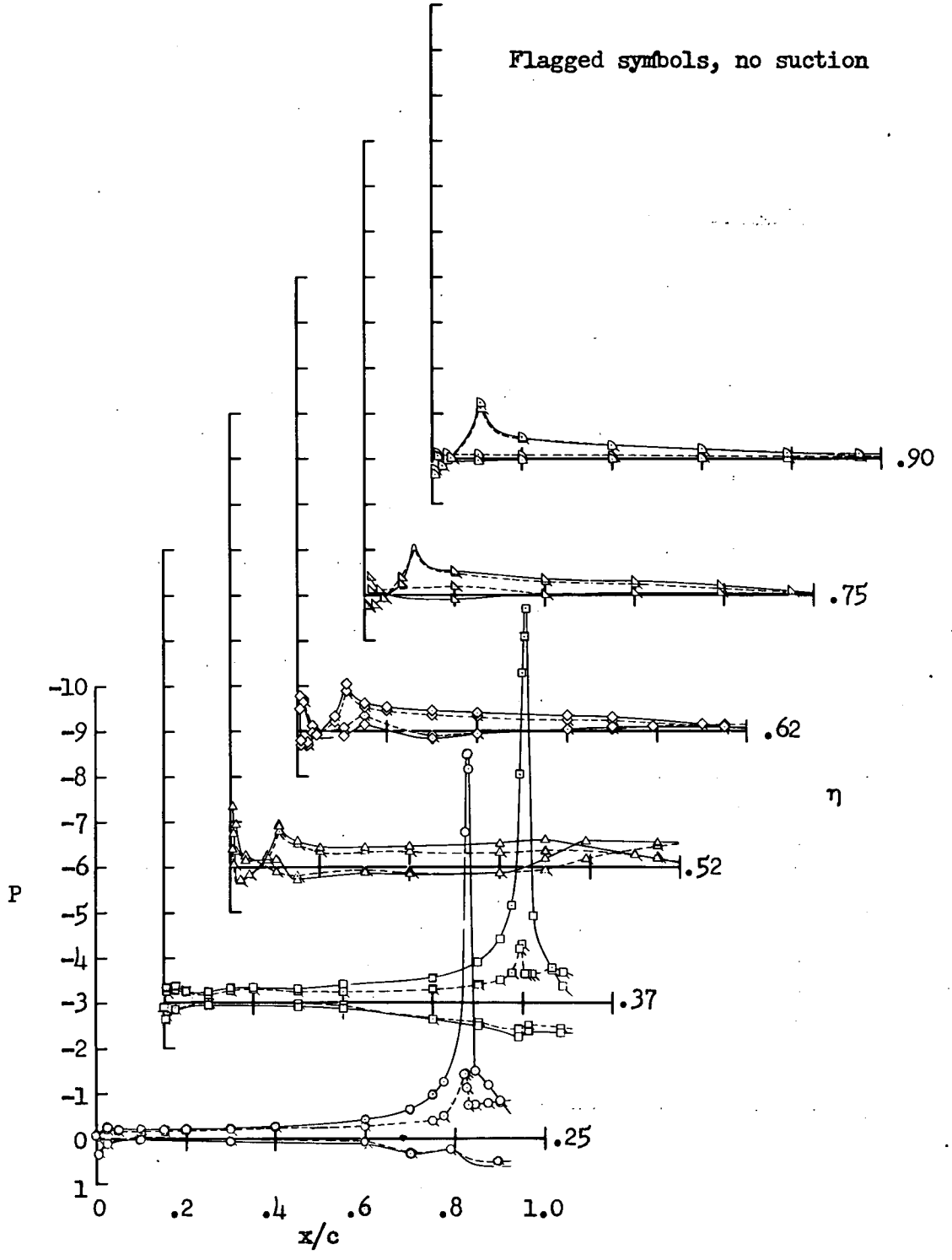

(a) $\alpha = 0.3^{\circ}$

Figure 17.- Chordwise pressure distributions on the wing with the part-span leading-edge flap (η = 0.40 to 1.0) deflected 40° and with the small-span trailing-edge flap (η = 0.21 to 0.46) deflected 60° with and without suction; side-inlet duct on.

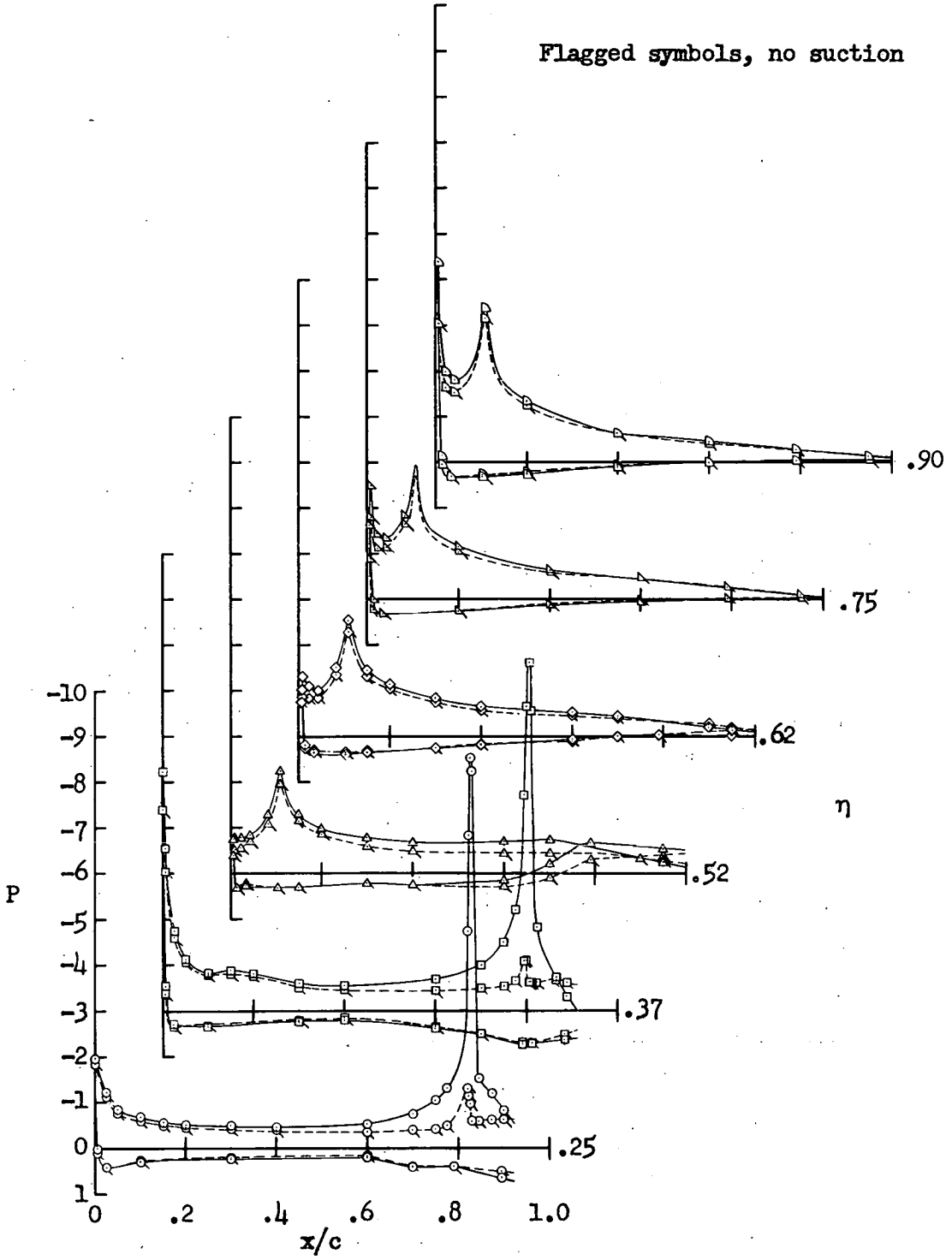

(b) $\alpha = 8.7^{\circ}$

Figure 17.- Continued.

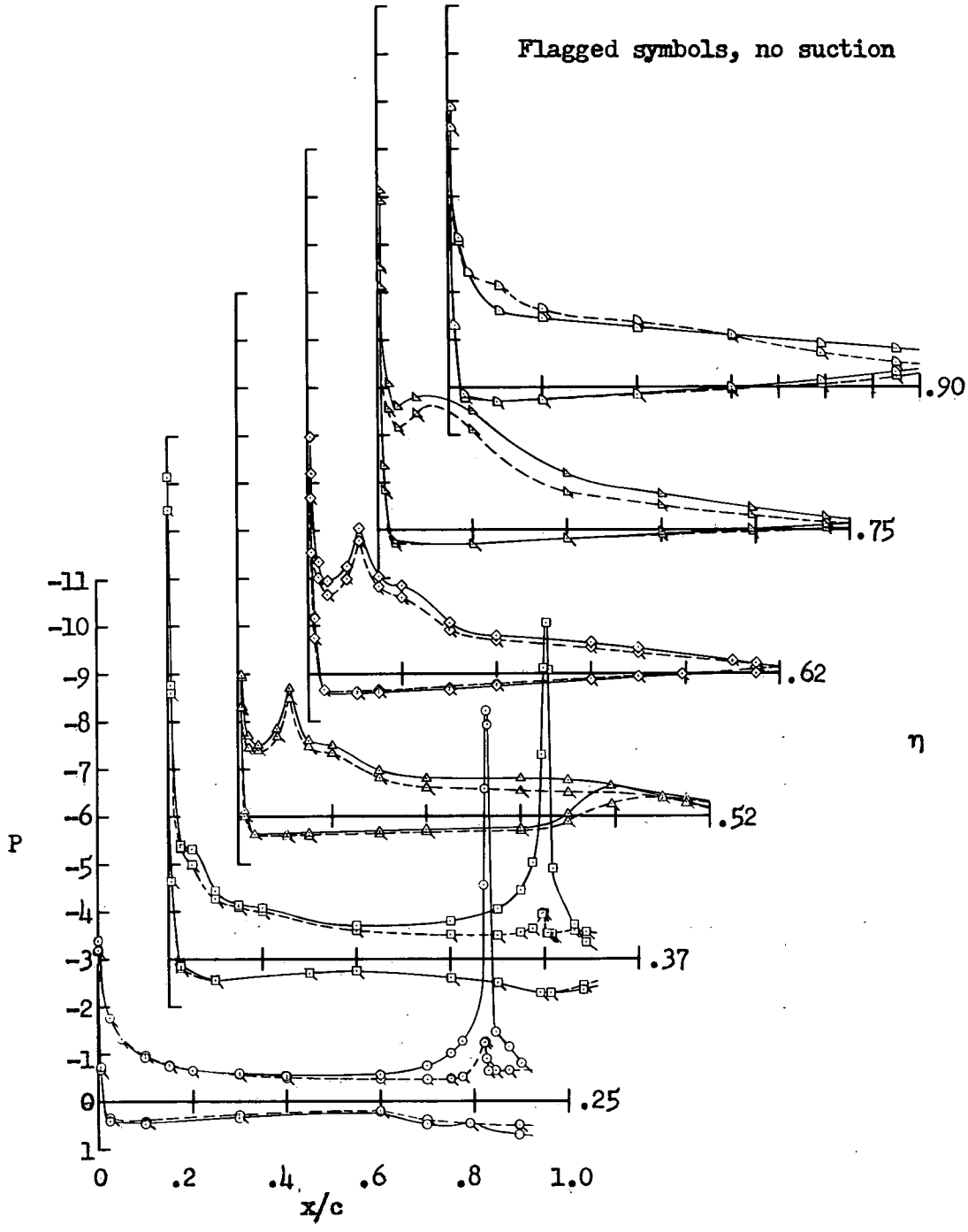

(c) $\alpha = 12.8^{\circ}$

Figure 17.- Continued.

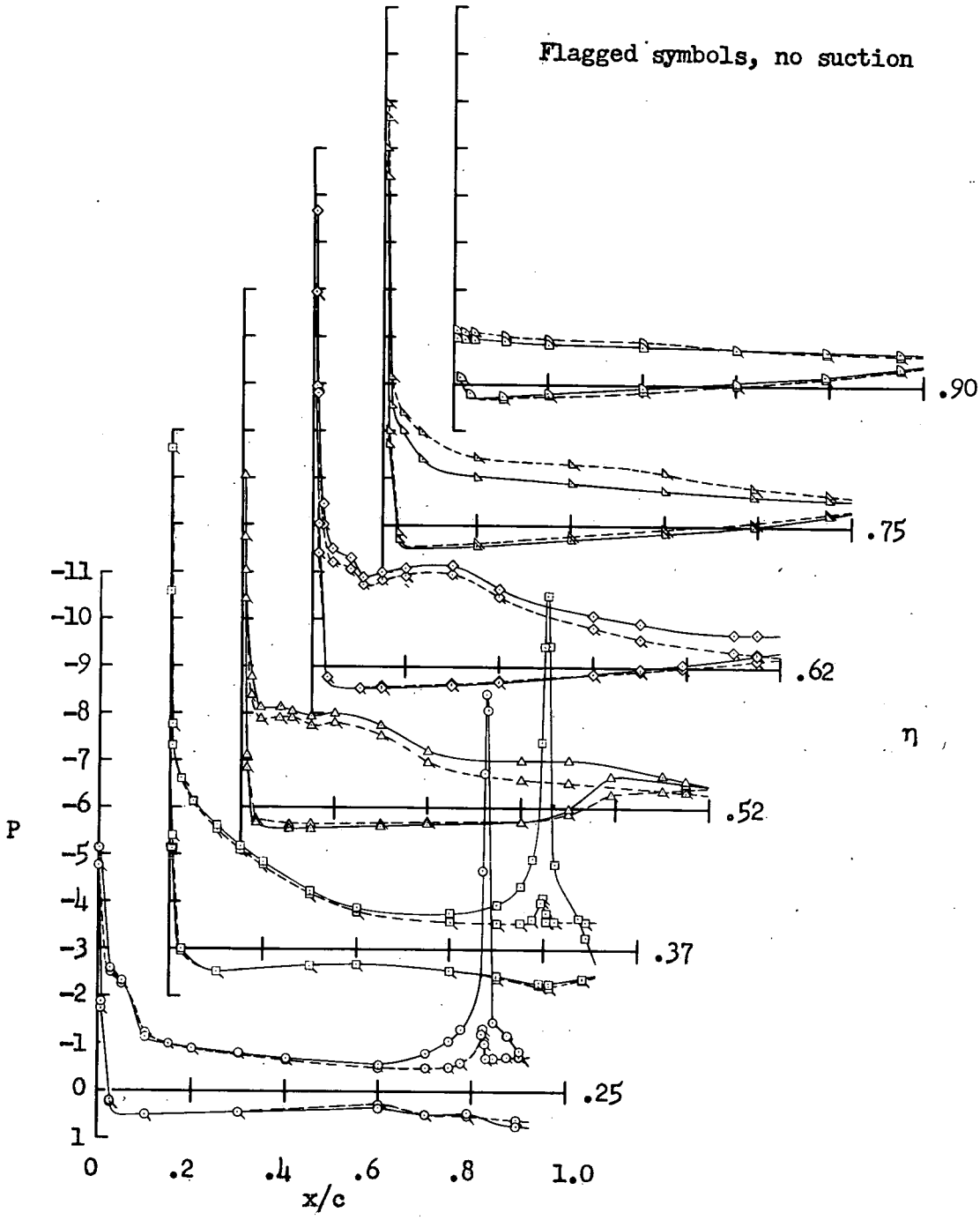

(d) $\alpha = 16.9^{\circ}$

Figure 17.- Continued.

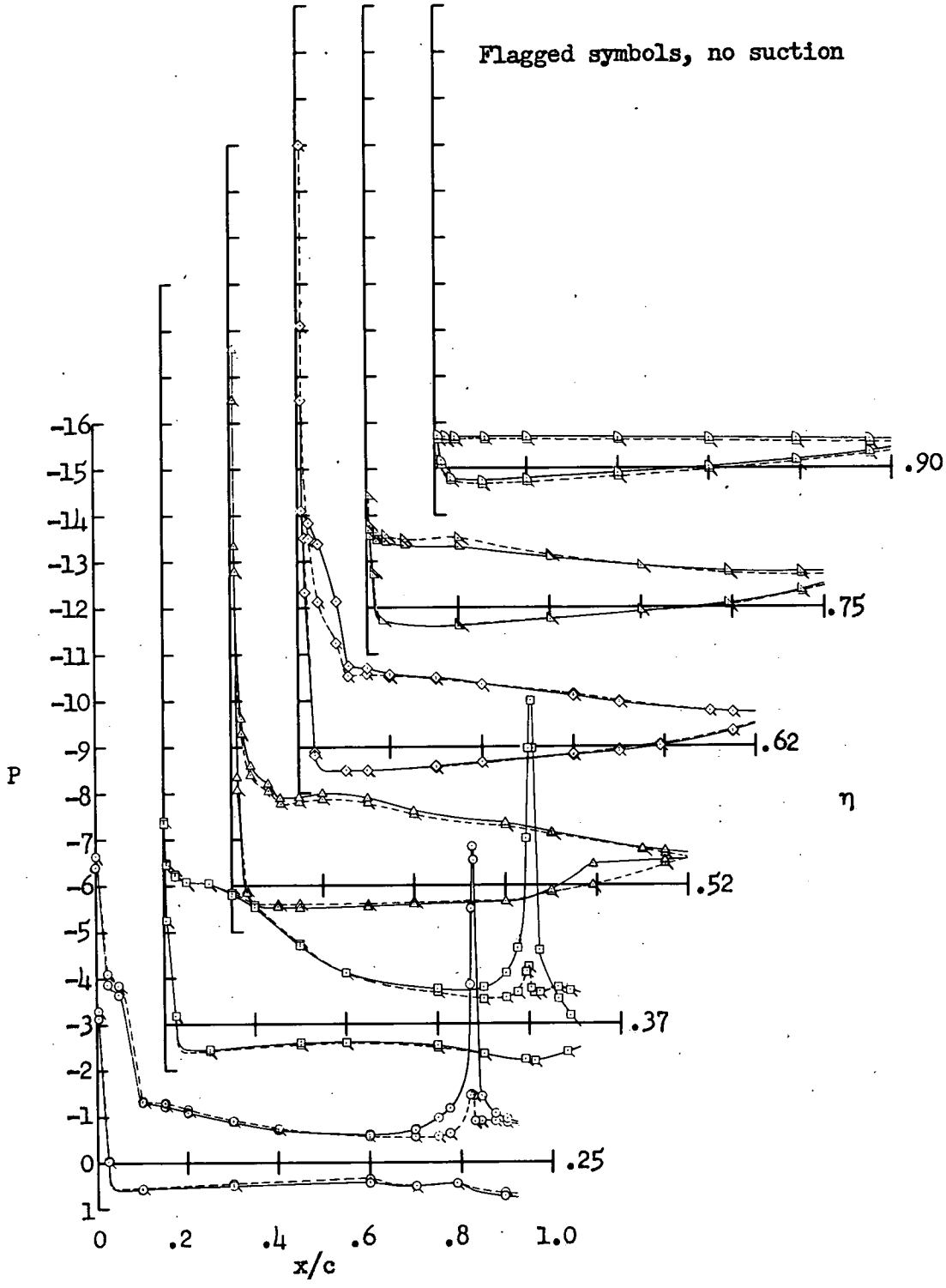

(e) $\alpha = 21.0^{\circ}$

Figure 17.- Concluded.

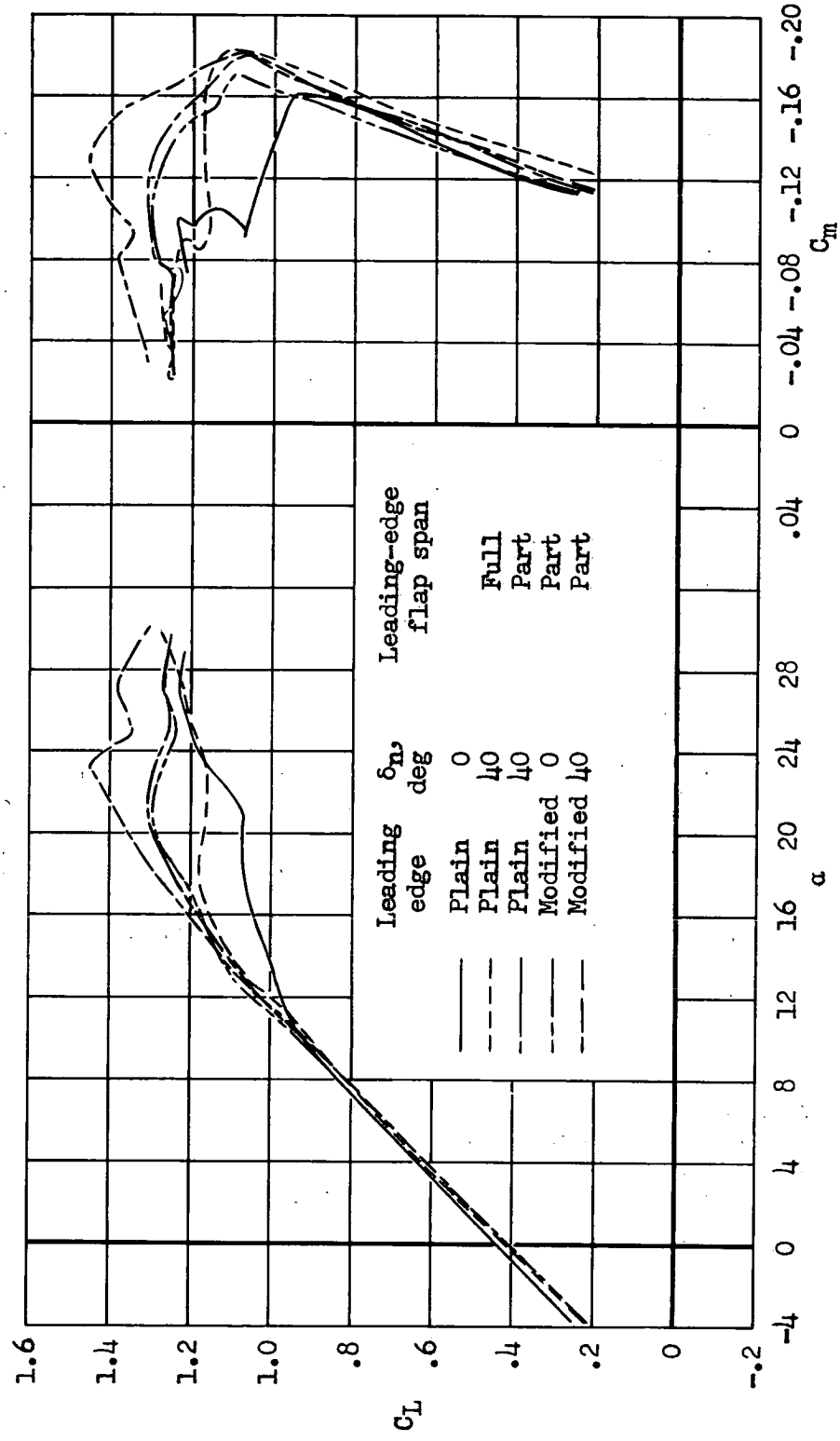

Figure 18.- A summary of the lift and pitching-moment characteristics of the model for the plain wing and several combinations of the modified leading edge (leading-edge radius 1.8-percent chord) and leading-edge flap configurations; tail off, side-inlet duct on, small-span trailing-edge flap (η = 0.21 to 0.46) deflected 60° with suction.

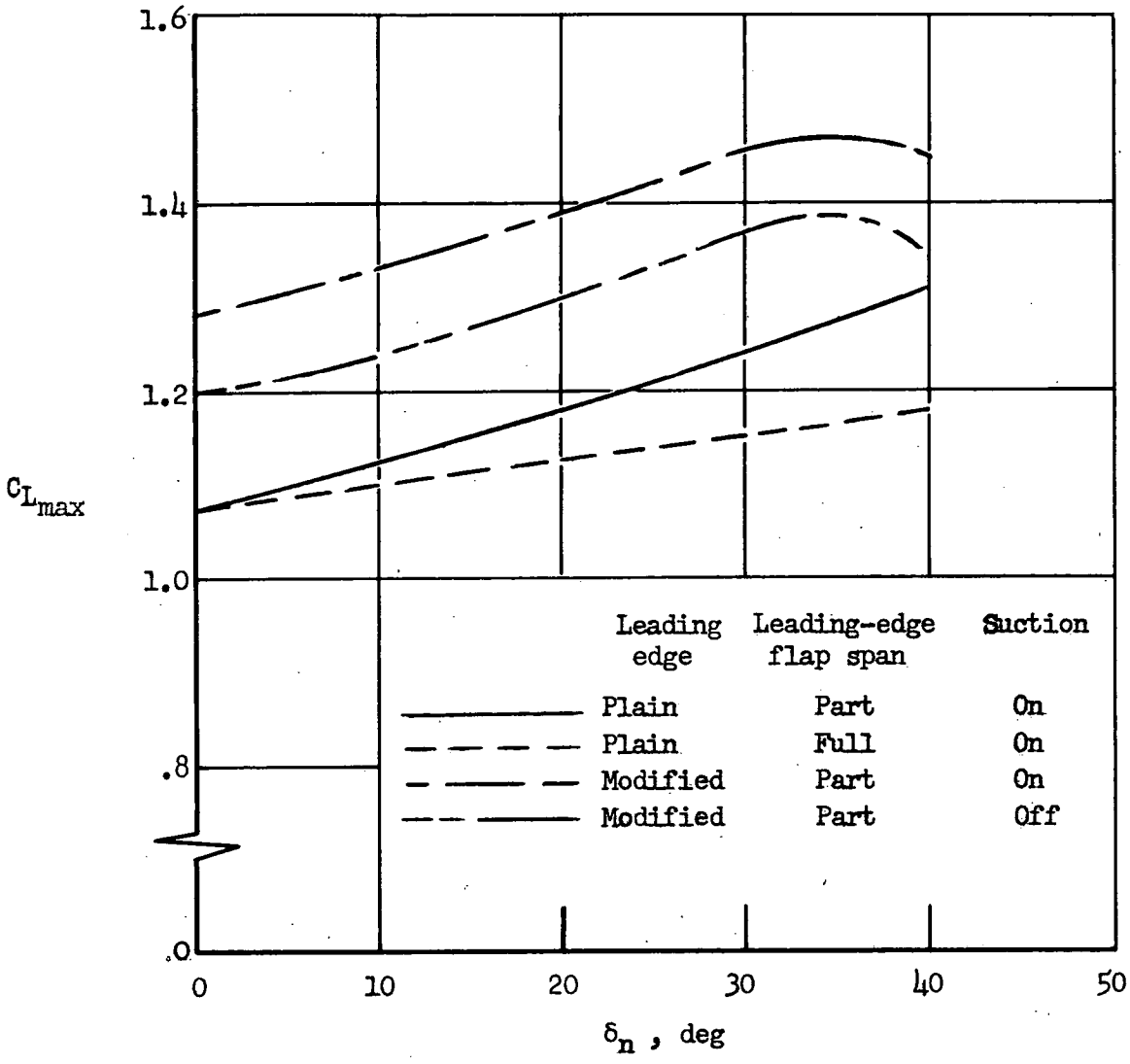

Figure 19.- The variation of maximum lift coefficient with leading-edge flap deflection; tail off, side-inlet duct on, small-span trailing-edge flap (η = 0.21 to 0.46) deflected 60° with suction. Modified leading edge had leading-edge radius of 1.8-percent chord for η = 0.40 to 1.0.

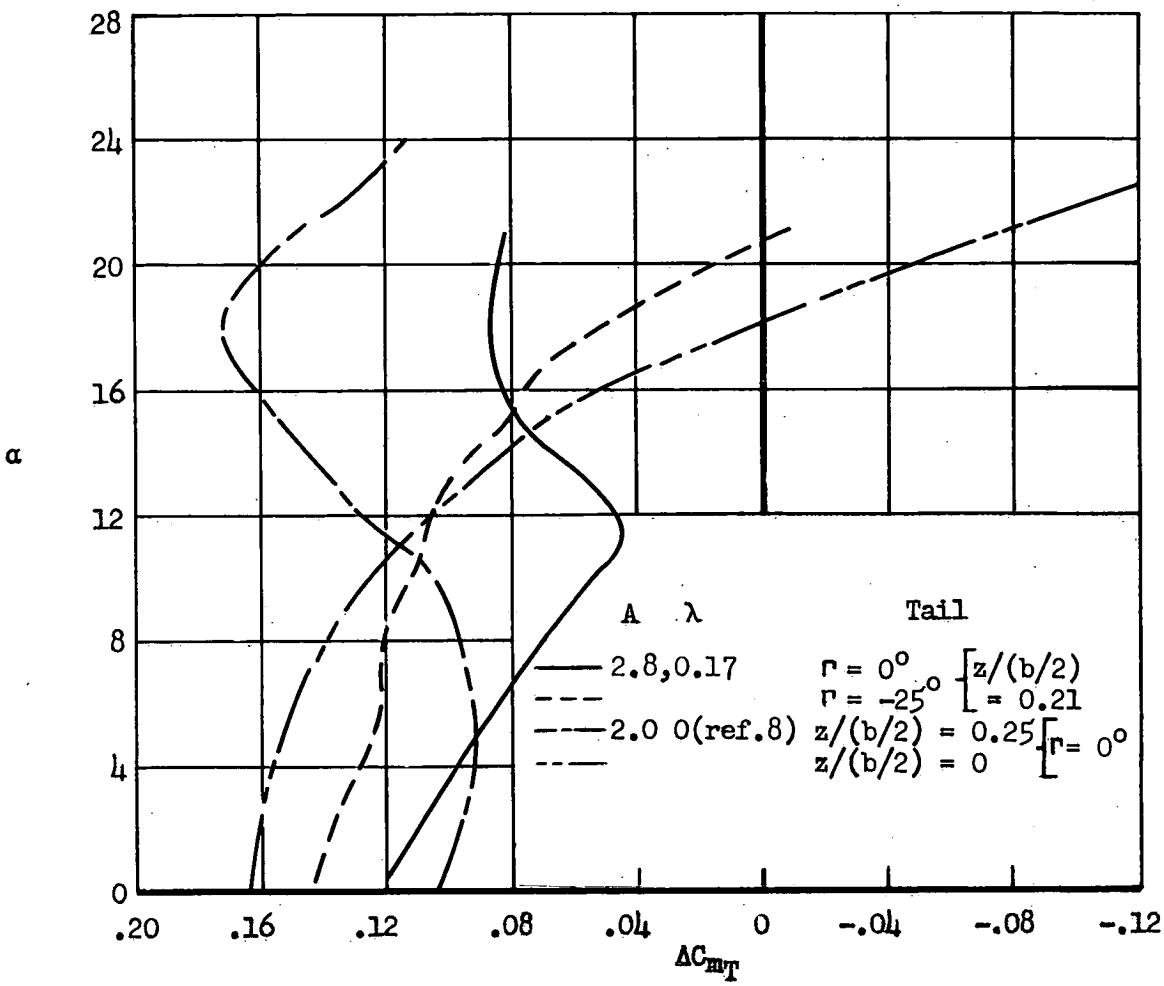

Figure 20.- Comparison of the effects of tail droop for the present model with those of tail height for a triangular-wing model on the pitching-moment contribution of the tail. For the present model, leading-edge flaps (part span) were deflected 40° and trailing-edge flaps were at 60° with suction. For the triangular-wing model, part-span slotted trailing-edge flaps were at 40° and no leading-edge flaps were used.

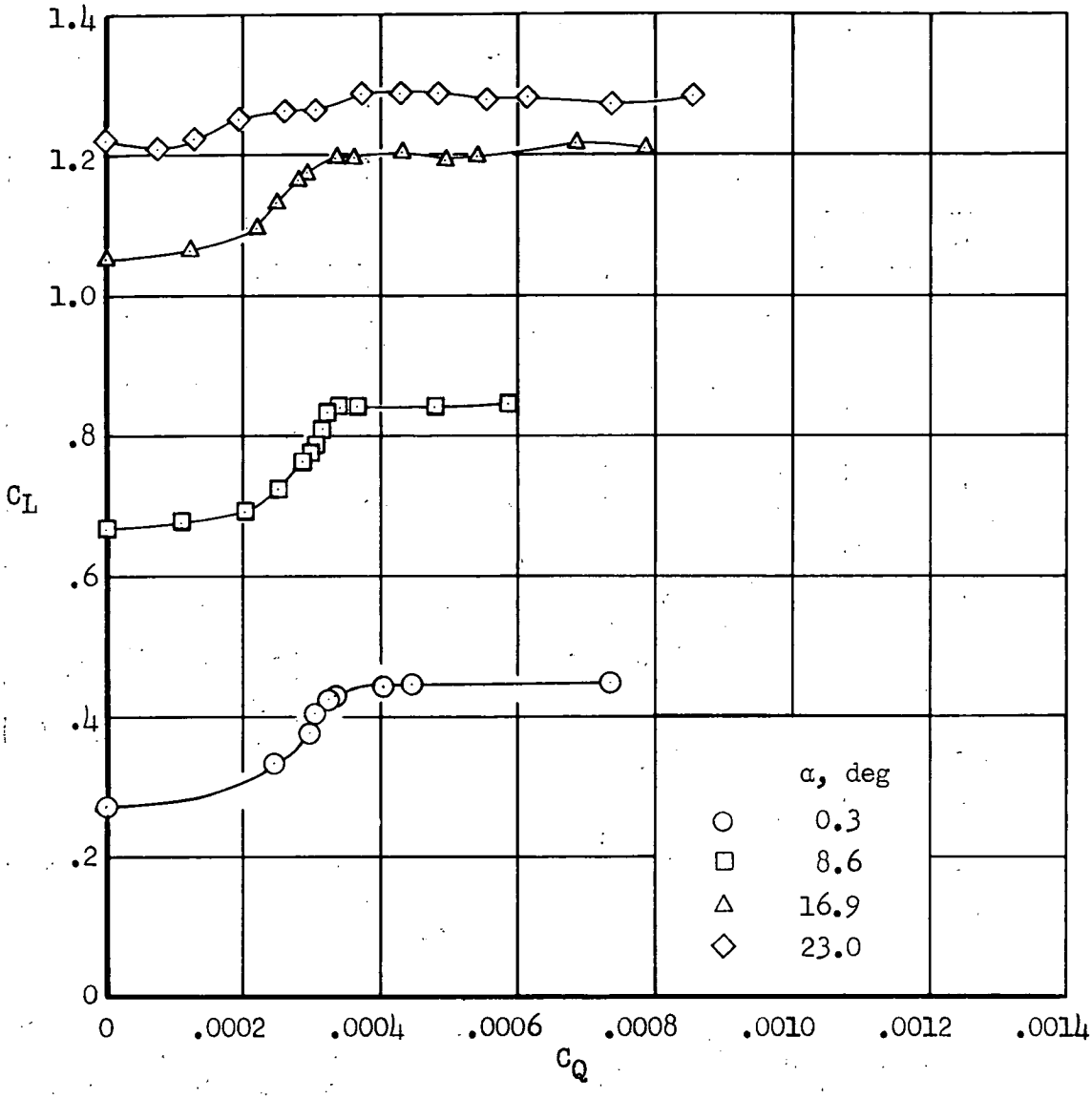

(a) Small-span flap; porous area 8.

Figure 21.- The effect of suction flow coefficient on lift coefficient for the trailing-edge flaps deflected 60°; side-inlet duct on, part-span leading-edge flap (η = 0.40 to 1.0) deflected 40°.

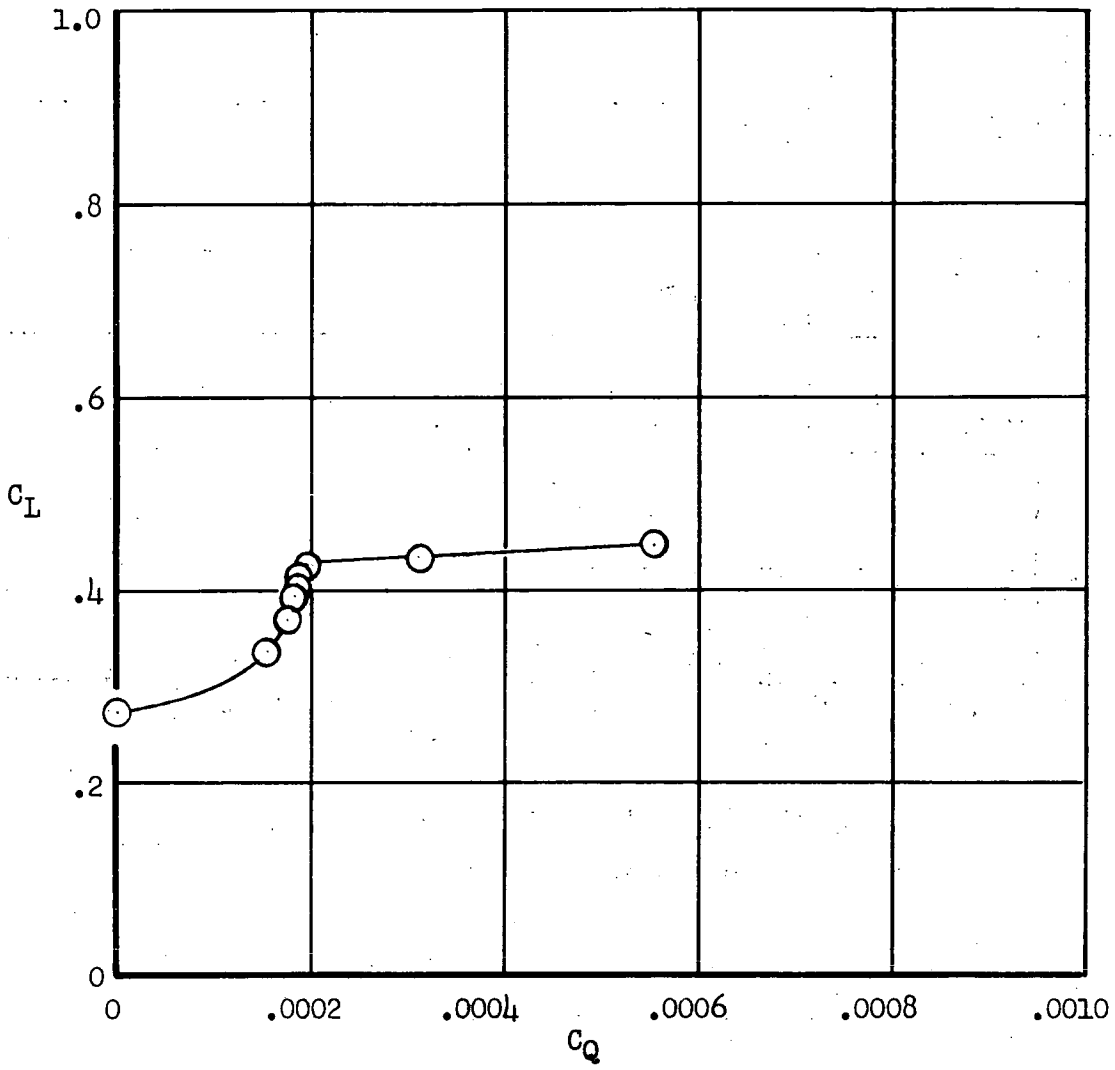

(b) Small-span flap; porous area 7; $\alpha = 0.3^\circ$.

Figure 21.- Continued.

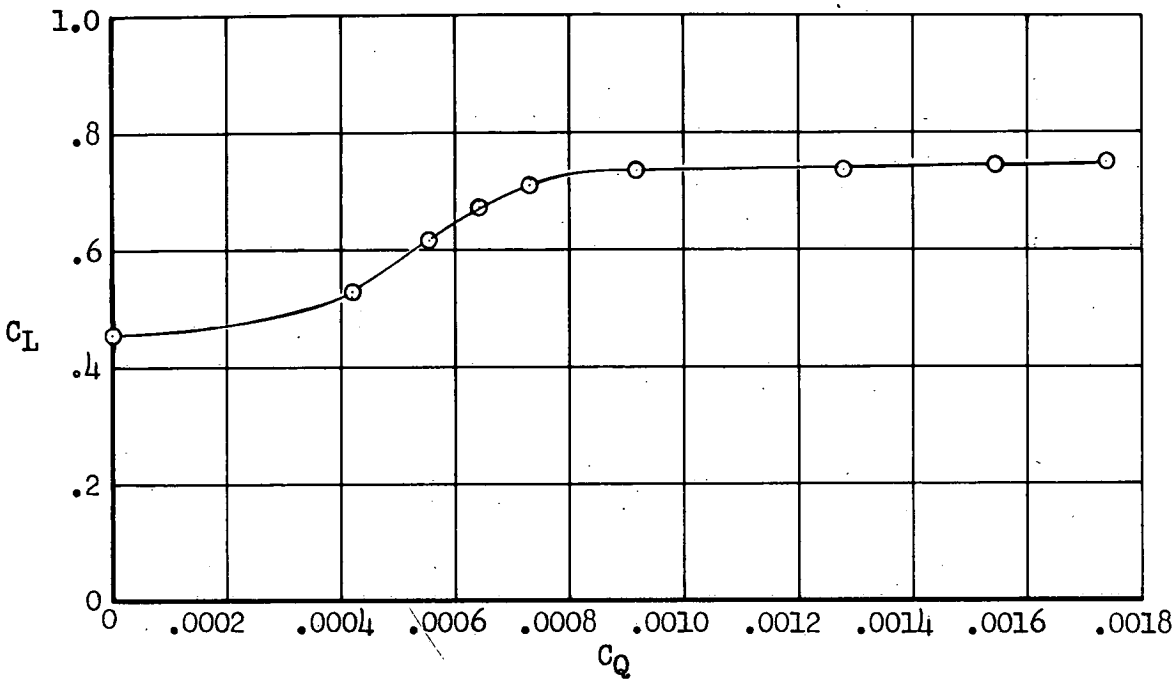

(c) Large-span flap; $\alpha = 0.7^\circ$.

Figure 21.- Concluded.

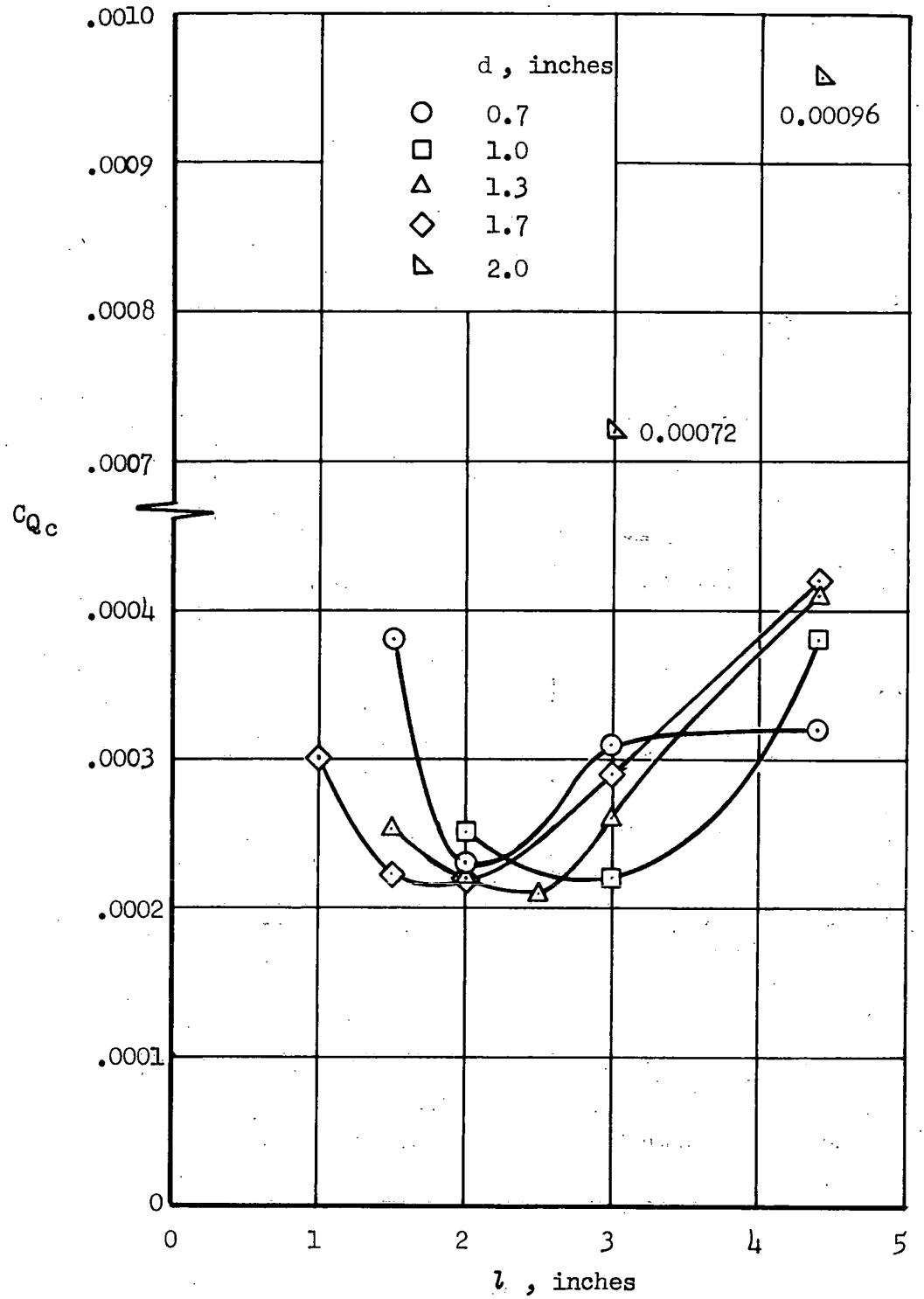

Figure 22.- The effect of porous-area extent and location on the critical flow coefficient for the small-span trailing-edge flap (η = 0.21 to 0.46) deflected 60°; side-inlet duct on, part-span leading-edge flap (η = 0.40 to 1.0) deflected 40°.

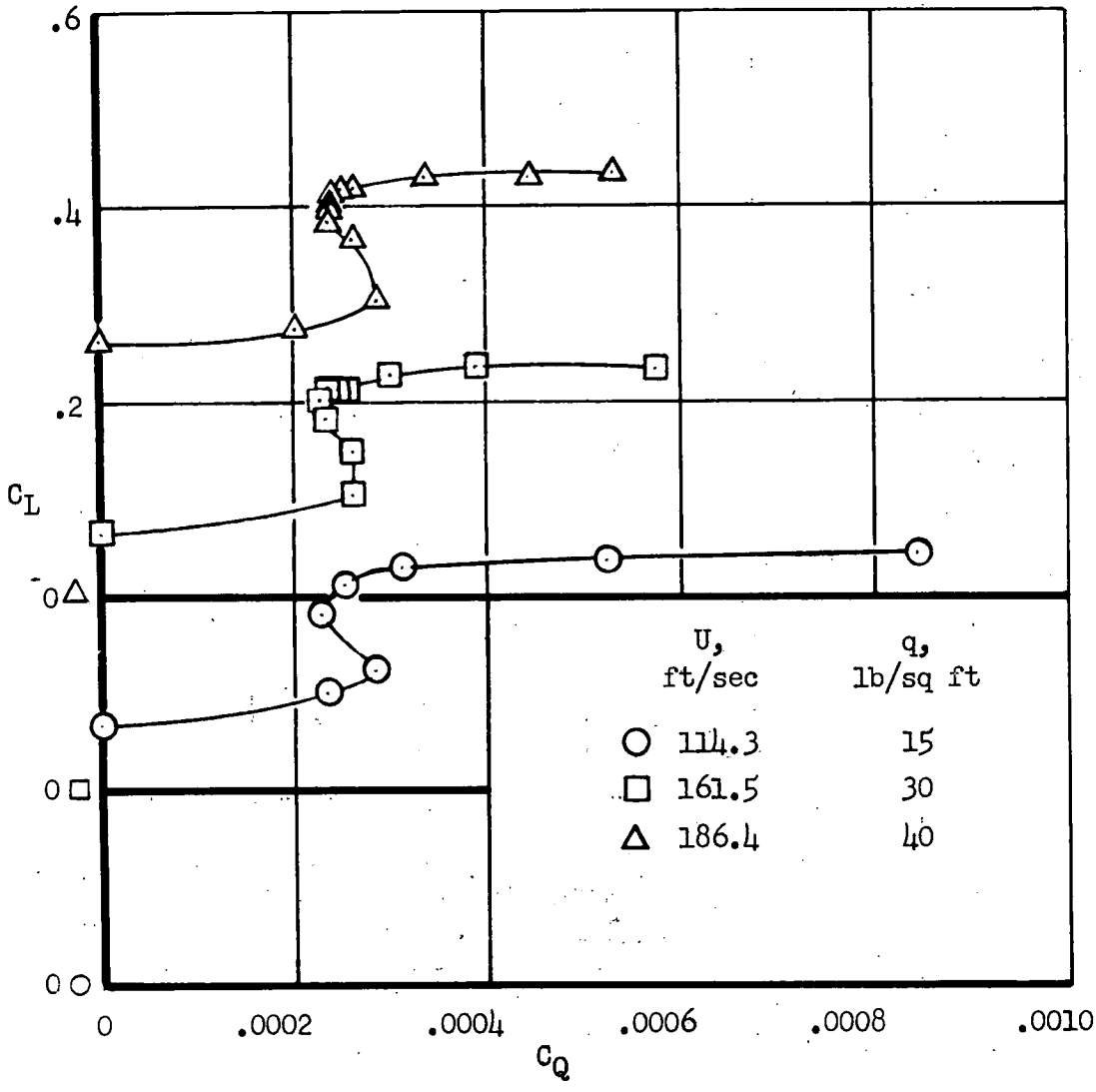

Figure 23.- The effect of streamwise velocity on the variation of lift coefficient with flow coefficient for the small-span flap (η = 0.21 to 0.46) deflected 60° with porous area 17; side-inlet duct on, part-span leading-edge flap (η = 0.40 to 1.0) deflected 40°, α = 0.3°.

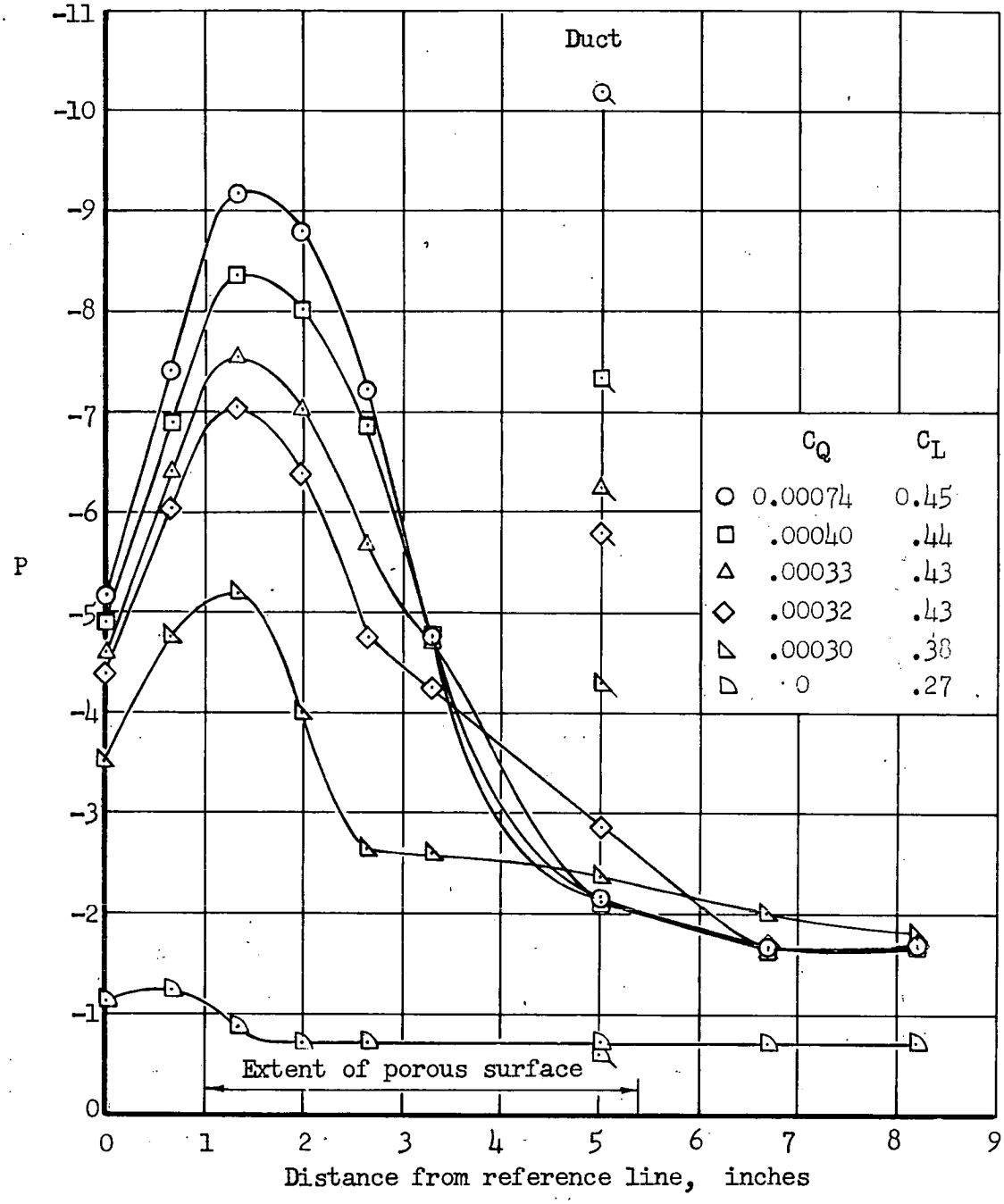

(a) $\eta = 0.25$

Figure 24.- The effect of duct pressure coefficient and flow coefficient on chordwise surface pressure distributions in the vicinity of the porous area of the small-span flap (η = 0.21 to 0.46) deflected 60°; side-inlet duct on, part-span leading-edge flap (η = 0.40 to 1.0) deflected 40°, porous area 8, $\alpha = 0.3°$.

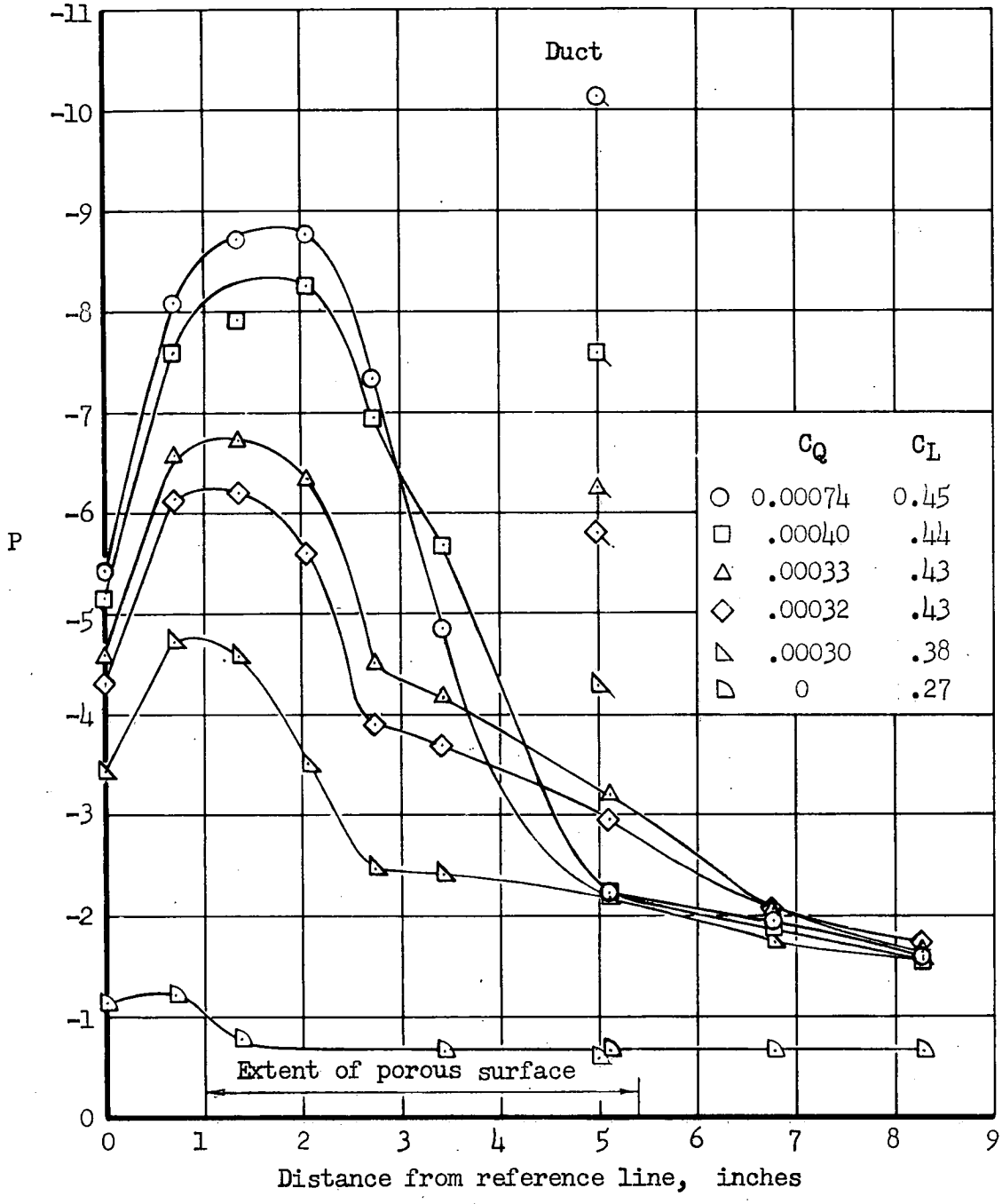

(b) $\eta = 0.37$

Figure 24.- Concluded.

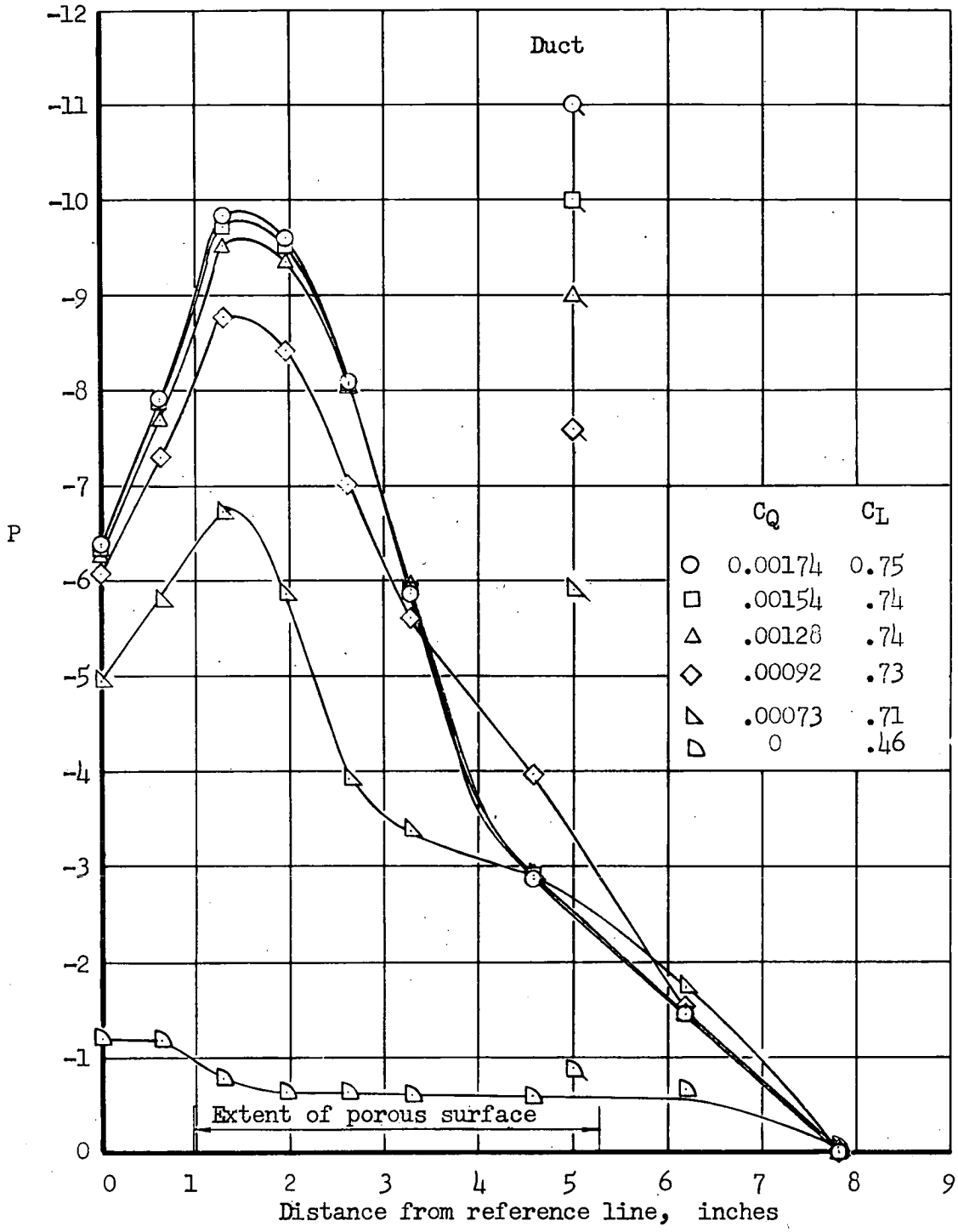

(a) Chordwise variation at $\eta = 0.52$.

Figure 25.- The effect of duct pressure coefficient and flow coefficient on chordwise and spanwise surface pressure distributions in the vicinity of the porous area of the large-span flap (η = 0.21 to 0.66) deflected 60°; side-inlet duct on, part-span leading-edge flap (η = 0.40 to 1.0) deflected 40°, $\alpha = 0.6°$.

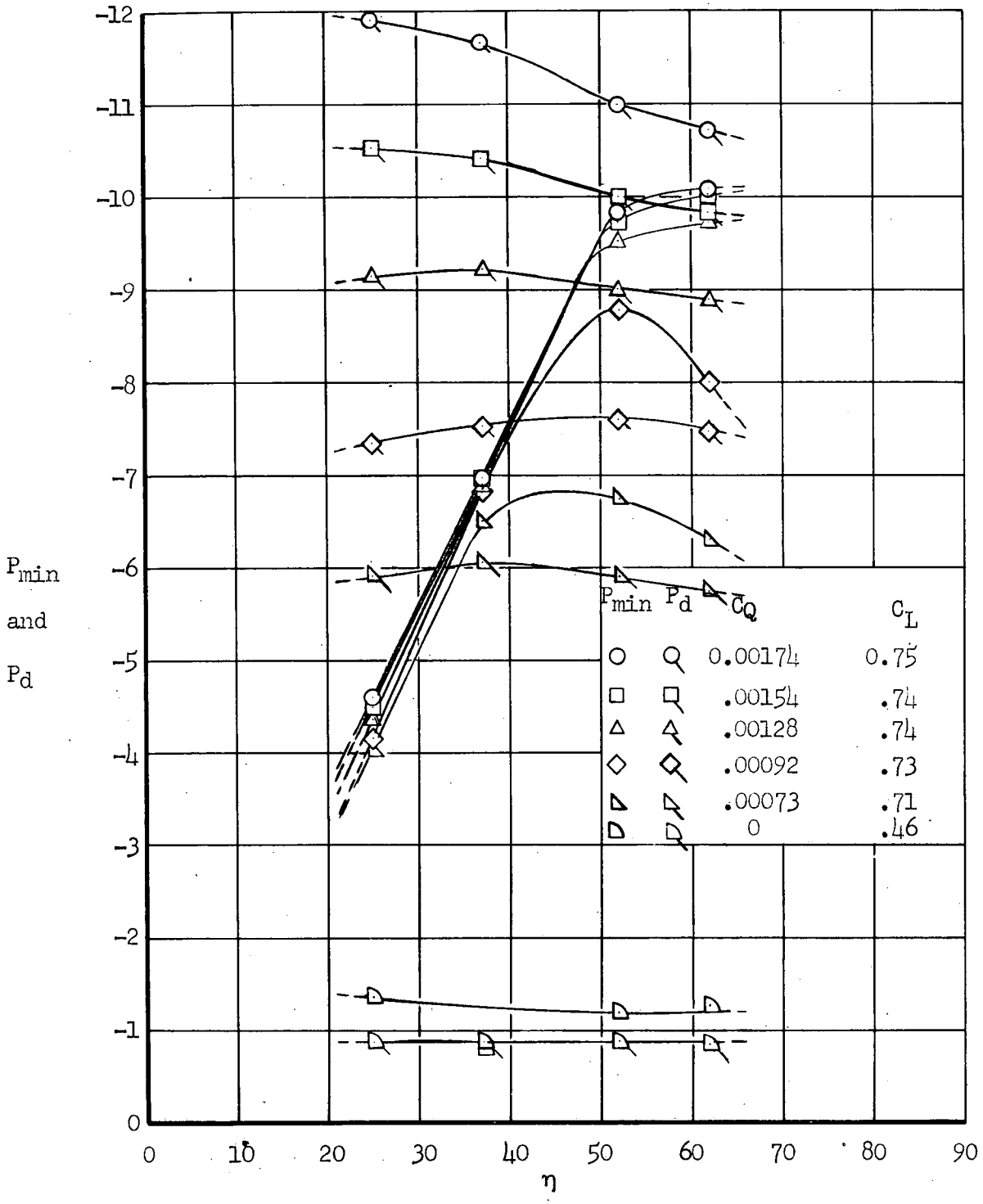

(b) Spanwise variation.

Figure 25.- Concluded.

NACA - Langley Field, Va.